IMMUNOLOGY

Engineering of hybrid spheroids of mesenchymal stem cells and drug depots for immunomodulating effect in islet xenotransplantation

Tiep Tien Nguyen[1,2], Duc-Vinh Pham[1], Junhyeung Park[1], Cao Dai Phung[1], Mahesh Raj Nepal[1], Mahesh Pandit[1], Manju Shrestha[1], Youlim Son[3], Mili Joshi[3], Tae Cheon Jeong[1], Pil-Hoon Park[1], Dong-Young Choi[1], Jae-Hoon Chang[1], Ju-Hyun Kim[1], Jae-Ryong Kim[3], Il-Kug Kim[3], Chul Soon Yong[1], Jong Oh Kim[1], Jong-Hyuk Sung[4,5], Hu-Lin Jiang[6,7,8,9], Hyung-Sik Kim[10,11], Simmyung Yook[2]*, Jee-Heon Jeong[1,12]*

Immunomodulation is an essential consideration for cell replacement procedures. Unfortunately, lifelong exposure to nonspecific systemic immunosuppression results in immunodeficiency and has toxic effects on non-immune cells. Here, we engineered hybrid spheroids of mesenchymal stem cells (MSCs) with rapamycin-releasing poly(lactic-*co*-glycolic acid) microparticles (RAP-MPs) to prevent immune rejection of islet xenografts in diabetic C57BL/6 mice. Hybrid spheroids were rapidly formed by incubating cell-particle mixture in methylcellulose solution while maintaining high cell viability. RAP-MPs were uniformly distributed in hybrid spheroids and sustainably released RAP for ~3 weeks. Locoregional transplantation of hybrid spheroids containing low doses of RAP-MPs (200- to 4000-ng RAP per recipient) significantly prolonged islet survival times and promoted the generation of regional regulatory T cells. Enhanced programmed death-ligand 1 expression by MSCs was found to be responsible for the immunomodulatory performance of hybrid spheroids. Our results suggest that these hybrid spheroids offer a promising platform for the efficient use of MSCs in the transplantation field.

INTRODUCTION

Immunomodulation therapy is an integral part of organ and cell replacement procedures as it prevents immune cells from attacking transplants and, thus, improves graft survival (*1*, *2*). Various systemic immunomodulatory therapeutics have been subjected to clinical trials, and some have exhibited potent effects (*2*). Unfortunately, lifelong exposure to this nonspecific immunosuppression results in immunodeficiency and has toxic effects on normal cells, and patients so affected can develop opportunistic infections, organ failures, or even life-threatening malignancies (*3*). Therefore, future efforts should focus on developing more effective therapies that circumvent aggressive immune responses and do not involve the prolonged systemic administration of high-dose immunosuppressants.

Mesenchymal stem cell (MSC) therapy has emerged as a potent immunosuppressive tool (*3*–*5*) because it effectively protects transplants from oxidative stress, has proregenerative properties, and modulates the immune system (*6*, *7*). The effects of MSCs are considered to be due to cell-cell contact and the secretion of various soluble paracrine factors (*3*). Although MSCs are often considered immune privileged (*8*), they express high levels of major histocompatibility molecules (MHCs) and activating natural killer (NK) cell receptors on their surface after encountering immune cells (*9*). As a consequence, MSCs are susceptible to lysis by T and NK cells, and this is responsible for the early rejection of MSCs in vivo (*10*). To achieve durable effects, multiple doses of MSCs must be administered to increase cell engraftment, but this substantially increases treatment costs and reduces patient compliance (*11*). Furthermore, recent evidence shows that treatment based on MSCs alone falls short of the demand for organ and cell replacement procedures (*11*).

Several strategies have been developed to improve MSC potency, including appropriate licensing of MSCs with inflammatory conditions and cotreatment with minimal doses of immunosuppressants (*12*–*17*). The inflammatory cytokine priming approach often leads to transient expression of various immunosuppressive molecules in MSCs and has been well demonstrated to be effective in vitro and animal models of several inflammatory diseases, but to date, it has not been demonstrated to enhance cell graft survival (*17*–*19*). On the other hand, the simultaneous administration of MSCs and immunosuppressive agents, such as rapamycin (RAP) offers the possibility of more durable immunosuppression. This method has been used to achieve tolerance in preclinical allogeneic cell (pancreatic islet) and organ (heart) transplantation models (*12*, *14*). However, multiple doses of systemically administered drugs show inconvenience and suboptimal efficacy due to drug distribution variability among recipients (*20*). Hence, there is still a need for an effective drug delivery system that boosts the immunomodulatory potency of MSCs in the context of organ/cell transplantation without the requirement for lifelong systemic immunosuppressants.

[1]College of Pharmacy, Yeungnam University, Gyeongsan, Gyeongbuk, 38541, Republic of Korea. [2]College of Pharmacy, Keimyung University, Daegu, 42601, Republic of Korea. [3]College of Medicine, Yeungnam University, Daegu, 42415, Republic of Korea. [4]College of Pharmacy, Yonsei Institute of Pharmaceutical Sciences, Yonsei University, Incheon, 21983, Republic of Korea. [5]Epibiotech Co. Ltd., Incheon, 21983, Republic of Korea. [6]State Key Laboratory of Natural Medicines, China Pharmaceutical University, Nanjing, 210009, China. [7]Jiangsu Key Laboratory of Druggability of Biopharmaceuticals, China Pharmaceutical University, Nanjing, 210009, China. [8]Jiangsu Key Laboratory of Drug Discovery for Metabolic Diseases, China Pharmaceutical University, Nanjing, 210009, China. [9]NMPA Key Laboratory for Research and Evaluation of Pharmaceutical Preparations and Excipients, China Pharmaceutical University, Nanjing, 210009, China. [10]Department of Life Science in Dentistry, School of Dentistry, Pusan National University, Yangsan, 50612, Republic of Korea. [11]Dental and Life Science Institute, Pusan National University, Yangsan, 50612, Republic of Korea. [12]Department of Precision Medicine, School of Medicine, Sungkyunkwan University, Suwon, 16419, Republic of Korea.
*Corresponding author. Email: jeeheon@skku.edu (J.-H.J.); ysimmyung@kmu.ac.kr (S.Y.)

In this study, we report an effective methodology to potentiate the immunomodulatory properties of MSCs via engineering hybrid spheroids with RAP-releasing poly(lactic-*co*-glycolic acid) (PLGA) microparticle depots (RAP-MPs). The devised hybrid spheroids were locoregionally transplanted with rat pancreatic islets into diabetic C57BL/6 mice to prevent the strong immune rejection of these xeno-sourced islets. This approach only required a single treatment with a low-dose immunosuppressant but resulted in long-term effects on immunosuppression (*21*). Encouraged by the first European Union–approved allogeneic adipose-derived MSC preparation (darvadstrocel; NCT01541579; TiGenix) for Crohn's disease, we believe that our approach constitutes a promising means of efficiently using stem cells in the transplantation field and for the treatment of various inflammatory diseases (*22*).

RESULTS

Characterization of RAP-MPs

RAP-MPs were fabricated using oil-in-water emulsification. Scanning electron microscopy (SEM) revealed that RAP-MPs had smooth surfaces and sizes ranging from 1 to 8 μm (average 4.4 ± 1.7 μm; Fig. 1, A and B). RAP was found to be physically encapsulated in PLGA microparticles as no new peaks were observed in Fourier transform infrared spectroscopy (FTIR) of RAP-MPs as compared with blank-MPs (Fig. 1C). Mean loading capacity and encapsulation efficiency of RAP-MPs, as determined by high-performance liquid chromatography (HPLC), were 4.10 ± 0.26% and 82.0 ± 5.2%, respectively. Notably, RAP-MPs exhibited a sustained release pattern of RAP for ~30 days, with minimal burst release during the first 2 days (Fig. 1D).

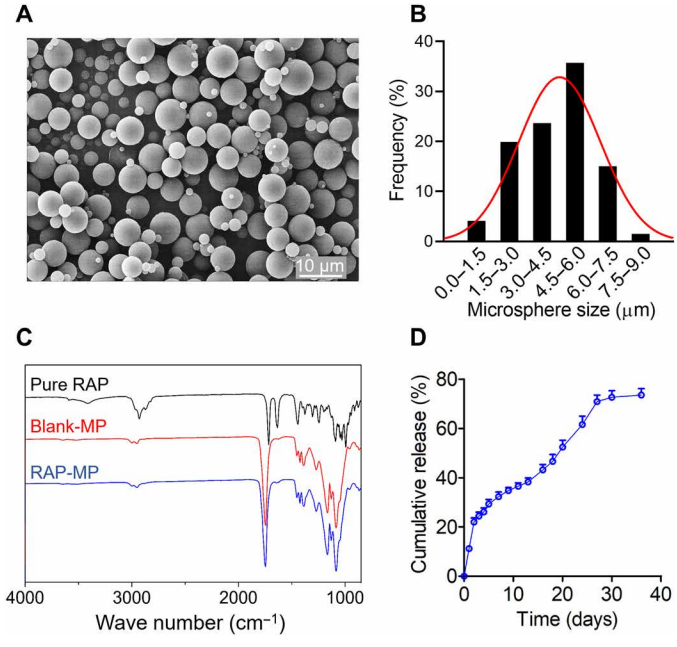

Fig. 1. Characterization of RAP-MPs. (**A**) Representative SEM image of RAP-MPs. (**B**) Size distribution of RAP-MPs. More than 200 particles were measured. (**C**) FTIR of pure RAP powder (black line), blank-MPs (red line), and RAP-MPs (blue line). (**D**) In vitro release profile of RAP from RAP-MPs incubated in phosphate-buffered saline [PBS (pH 7.4) plus 1% Tween 20] at 37°C and 150 rpm. Samples ($n = 3$) were regularly collected over 35 days.

Characterization of mouse adipose tissue–derived MSCs

MSCs were isolated from subcutaneous adipose tissues of C57BL/6 mice, as previously described (*23*). Isolated MSCs had a typical fibroblast-like shape and were positive (≥95%) for the MSC markers (CD29, CD44, CD90, and Sca-1) and negative (<2%) for CD11b, CD34, and CD45 (fig. S1A). In addition, these MSCs had the ability to differentiate into the osteogenic lineage as demonstrated by the deposition of alizarin red S–stained calcium nodules, into the adipogenic lineage as demonstrated by the accumulation of oil red O–stained lipid droplets, and into the chondrogenic lineage as demonstrated by the accumulation of Alcian blue–stained glycosaminoglycans (fig. S1B).

Rapid formation of uniform MSC spheroids in methylcellulose solution

An illustration of the fabrication of spheroids in high viscosity methylcellulose solution is provided in Fig. 2A. Free water molecules were rapidly absorbed by the methylcellulose solution after injecting a suspension concentrate containing MSCs and RAP-MPs. This led to the close contact between MSCs and RAP-MPs and facilitated the spontaneous and stable formation of cell-particle hybrid spheroids within 2 hours. In this study, each spheroid was constructed from ~2.5×10^4 MSCs and various amounts of RAP-MPs theoretically equivalent to 10, 40, 100, and 200 ng of RAP, which is referred to as HS10, HS40, HS100, and HS200, respectively. Spheroids without RAP-MPs are referred to as non–RAP-MP spheroids. The sizes of these spheroids were not detectably different. Immediately after construction, non–RAP-MP and HS100 spheroids were 740 ± 47 and 744 ± 32 μm in diameter, respectively ($P = 0.6849$; fig. S2, A and B). Meanwhile, the size of spheroids reduced by ~1.5-fold after 3 days in culture as a result of increased cell-cell contraction (non–RAP-MP spheroids: 492 ± 32 μm and HS100 spheroids: 478 ± 21 μm; Fig. 2, B and C, and fig. S2, C and D).

Next, we explored the distribution of RAP-MPs in hybrid spheroids after 3 days in culture. To this purpose, RAP-MPs were labeled with coumarin-6 (green fluorescence), and cell nuclei were stained blue with Hoechst 33342. A confocal laser scanning microscopy (CLSM) image of HS100 spheroid presented in Fig. 2D indicated that RAP-MPs were uniformly dispersed within spheroid. In addition, SEM revealed that spheroids were highly compact, and that RAP-MPs (red arrows) were clearly distinguished from the cell matrix (Fig. 2E and fig. S2E). The densities of RAP-MPs in hybrid spheroids were well correlated with their initial loadings (fig. S2E).

Liquid chromatography–tandem mass spectrometry (LC-MS/MS) was used to determine actual RAP loadings in hybrid spheroids. It was found that each spheroid in HS10, HS40, HS100, and HS200 spheroid groups contained 9.46 ± 1.08 ng [entrapment efficiency (EE) = 94.6 ± 10.8%], 38.34 ± 4.54 ng (EE = 95.8 ± 11.4%), 98.08 ± 10.98 ng (EE = 98.1 ± 11.0%), and 216.79 ± 17.21 ng (EE = 108.4 ± 8.6%) of RAP, respectively (Fig. 2F and fig. S2F). Next, release patterns of RAP from hybrid spheroids were examined. A similar RAP release profile was found in all groups, regardless of initial RAP-MP loading. In particular, 50 to 70% of RAP was released in the first week and 10 to 20% in the second week, and RAP release was almost exhausted after 3 weeks (Fig. 2F and fig. S2G). RAP release was more rapid from hybrid spheroids than from RAP-MP suspensions (Fig. 1D).

The fabrication of large-sized spheroids often raises the issue of cell viability due to nutrient and oxygen restrictions. To demonstrate

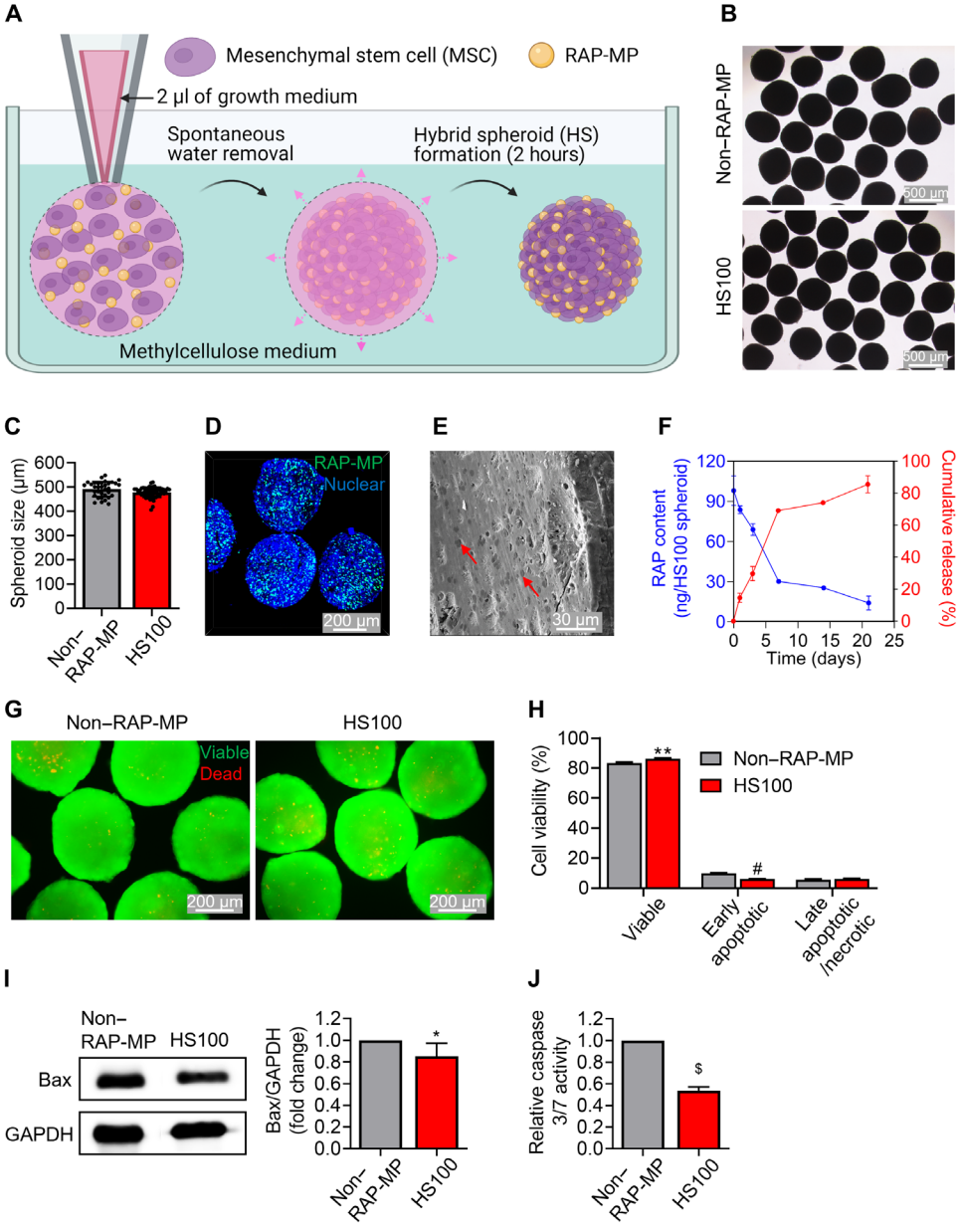

Fig. 2. Methylcellulose-based fabrication of hybrid spheroids of MSCs with RAP-MPs. (**A**) A schematic diagram of the fabrication process. Spheroids were retrieved from methylcellulose solution after incubation for 2 hours, cultured in MEM-α growth medium on nonadherent petri dishes, and assessed on day 3. Hybrid spheroids theoretically contained 2.5×10^4 MSCs and RAP-MPs equivalent to 100 ng of RAP per spheroid, which are referred to as HS100 spheroids. Spheroids without RAP-MPs are referred to as non–RAP-MP spheroids. (**B** and **C**) Morphologies and sizes of non–RAP-MP and HS100 spheroids. Scale bars, 500 μm. (**D**) Distribution of coumarin-6–labeled RAP-MPs in HS100 spheroids as determined by confocal laser scanning microscopy (CLSM). Cell nuclei were stained blue with Hoechst 33342. Scale bar, 200 μm. (**E**) SEM of HS100 spheroid. The red arrows indicate RAP-MPs. Scale bar, 30 μm. (**F**) Actual contents of RAP in HS100 spheroids with respect to culture time and cumulative RAP release percentages ($n = 3$ to 5). RAP contents in the samples were determined using the developed liquid chromatography–tandem mass spectrometry (LC-MS/MS) method. (**G** and **H**) Assessment of MSC viability in spheroids as determined by live/dead staining assay and flow cytometry–based quantitative assay, respectively. Scale bars, 200 μm. (**I** and **J**) Assessment of apoptotic events in spheroids based on Western blot determination of Bax level ($n = 6$ independent experiments) and determination of caspase 3/7 activity ($n = 3$ independent experiments), respectively. Data in (H), (I), and (J) are expressed as the means ± SDs and were analyzed using the unpaired two-tailed *t* test, $^*P < 0.05$, $^{**}P < 0.01$, $\#P < 0.001$, and $\$P < 0.0001$.

the superiority of our developed spheroid fabrication method, cell viability and apoptosis events were evaluated. A live/dead staining assay performed 3 days after spheroid fabrication in methylcellulose medium revealed that spheroids maintained high cell viability, which contrasted with the low viability observed when spheroids were produced using the hanging drop technique (Fig. 2G and fig. S3A). Quantitatively, the percentages of viable cells in monolayer [two-dimensional (2D)]–cultured MSCs and in non–RAP-MP spheroids fabricated using methylcellulose medium and hanging drop were 85.8 ± 0.9%, 83.4 ± 0.6% ($P = 0.0176$ versus 2D-MSC) and 66.1 ± 2.8%

(P = 0.0003 versus 2D-MSC), respectively (Fig. 2H and fig. S3B). In addition, we found that cell viability in HS100 spheroids (86.3 ± 0.4%) was slightly improved as compared to non–RAP-MP spheroids (P = 0.0027; Fig. 2H). Moreover, apoptotic protein markers, Bax and caspase 3/7, were evaluated using Western blot and a caspase activity assay, respectively. The results showed that MSCs in spheroids expressed significantly lower levels of these apoptotic protein markers than those in 2D-MSCs (fig. S4). Notably, RAP-MP incorporation in spheroids further decreased the apoptotic protein levels dose-dependently, although no remarkable change in viable and apoptotic cell numbers was observed among hybrid spheroids (Fig. 2, I and J, and fig. S5).

Immune-related gene expression profiling in hybrid spheroids

Spheroidal MSCs have been well documented to have better immunomodulatory effects than 2D-MSCs (*24*, *25*). Initially, we examined the dynamic expressions of immune-related genes in non–RAP-MP spheroids by quantitative reverse transcription polymerase chain reaction (qRT-PCR). Non–RAP-MP spheroids were fabricated and cultured in minimum essential medium–α (MEM-α) growth medium for 1 to 3 days (fig. S6). The expressions of *CD86*, *MHC-I*, *MHC-II*, *TGFB1*, *IL1RN*, and *IL4* were found to significantly increase with culture time. Only transient increases were observed in *INOS* and *HO-1* gene expressions after culture for 1 day. In contrast, the expressions of *PD-L1*, *COX-2*, and *IL6* in non–RAP-MP spheroids significantly decreased after 3 days of culture. Next, spheroids were treated with a cytokine cocktail containing interferon-γ (20 ng/ml; IFN-γ) and tumor necrosis factor–α (10 ng/ml; TNF-α) to mimic inflammatory events after spheroid transplantation. Exposure of spheroids to the cytokine cocktail for 3 days resulted in the profound up-regulations of the gene expression levels of *IDO1* (69.5 ± 19.4-fold, P = 0.0036), *INOS* (5.4 ± 0.5-fold, P = 0.0015), *PD-L1* (6.9 ± 2.9-fold, P = 0.0227), and *MHC-I* (8.5 ± 2.2-fold, P = 0.0044; Fig. 3 and fig. S7).

The effect of RAP-MP incorporation in hybrid spheroids on immune-related gene expression was further investigated. Non–RAP-MP and HS100 spheroids were cultured in MEM-α growth medium with or without cytokine cocktail supplementation (Fig. 3). In the absence of the cytokine cocktail, the gene expressions of *COX-2*, *IL6*, *TGFB1*, and *PD-L1* were significantly up-regulated in HS100 spheroids versus non–RAP-MP spheroids by 2.3 ± 0.5-fold (P = 0.0102), 3.6 ± 0.4-fold (P = 0.0005), 3.1 ± 0.8-fold (P = 0.0096), and 1.4 ± 0.1-fold (P = 0.0001), respectively, after 3 days in culture. Notably, cytokine exposure further increased the gene expressions of *MHC-I*, *IL10*, and *PD-L1* in HS100 spheroids by 1.5 ± 0.3-fold (P = 0.0318), 1.7 ± 0.1-fold (P < 0.0001), and 2.0 ± 0.1-fold (P < 0.0001), respectively. However, the gene expression levels of *IDO1* and *INOS* after 3 days in culture were substantially decreased by 1.9 ± 0.5- and 1.3 ± 0.1-fold, respectively, as a result of RAP-MP incorporation.

Effects of hybrid spheroids on islet functionality and islet xenograft survival

To determine the effect of spheroids on islet functionality, a glucose-stimulated insulin secretion (GSIS) assay was performed in a coculture system of islets and spheroids. As a result, there was no significant difference in insulin secretion by control islets and islets cocultured with spheroids at different RAP doses, confirming the biocompatibility of our developed spheroids on islet functionality (fig. S8).

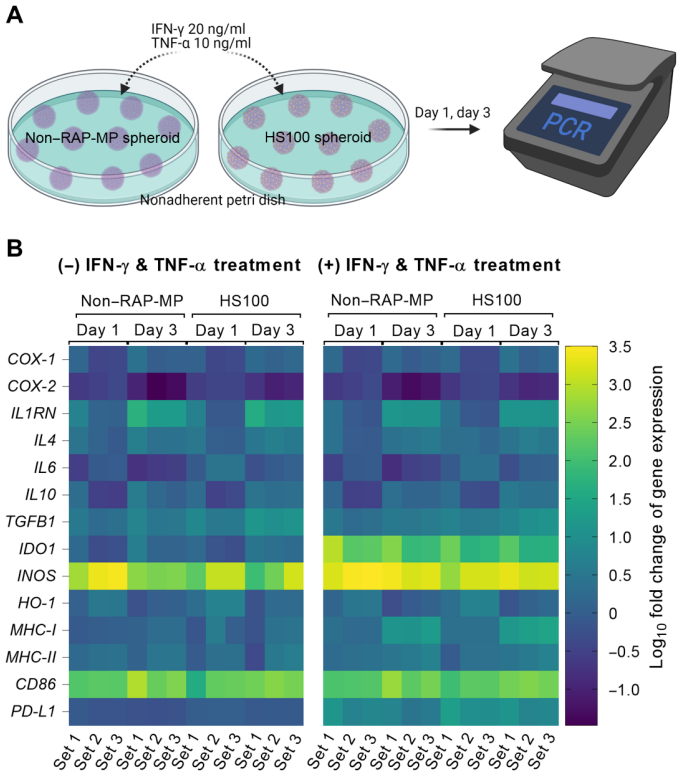

Fig. 3. Assessment of dynamic changes in immune-related gene expressions in spheroids. (**A**) Graphical illustration of spheroid culture, treatment, and assessment. Non–RAP-MP and HS100 spheroids were cultured in MEM-α growth medium with or without cytokine cocktail (IFN-γ and TNF-α) supplementation. Samples were collected and processed for qRT-PCR analysis after culture for 1 to 3 days. (**B**) Heatmap depiction of gene expression levels. Results are expressed as $\log_{10}$ fold changes versus day 0 (n = 3 independent experiments).

A pancreatic rat-to-mouse islet xenotransplantation model was established to develop strong immune reactions (*26*). Islets [400 islet equivalents (IEQs)] were transplanted alone (control) or with RAP-MPs, non–RAP-MP spheroids, or hybrid spheroids under the kidney capsules of streptozocin (STZ)–rendered diabetic C57BL/6 mice (Fig. 4A). Twenty spheroids, equivalent to 0.5 × 10^6 MSCs, were used per transplant. The doses of RAP per transplant in the RAP-MP, HS10, HS40, HS100, and HS200 spheroid groups were 1534.0 ± 499.8, 139.4 ± 24.2, 538.3 ± 24.6, 1378.2 ± 87.0, and 2882.2 ± 41.0 ng, respectively (P = 0.6225 for RAP-MP versus HS100 spheroid; fig. S9). Figure 4 (B and C) shows nonfasting blood glucose (NBG) levels of islet recipients (Fig. 4B) and Kaplan-Meier curves for xenograft survival times (Fig. 4C). As observed, islets in the control group were rejected rapidly with a median graft survival time (MST) of 9 days (means ± SD = 9.2 ± 0.8 days). The colocalization of islets with non–RAP-MP spheroids did not result in any improvement in islet survival with the MST of 7 days (means ± SD = 7.2 ± 1.8 days; P = 0.0518 versus islet control). Meanwhile, a local single dose of RAP-MP extended islet survival by about twofold over the islet control group to 18.5 days (means ± SD = 21.2 ± 7.5 days; P = 0.0008 versus control). However, no islet graft in the RAP-MP group was functional at 40 days after transplantation.

Notably, locoregional hybrid spheroids effectively protected islet xenografts from early immune rejection in a RAP dose-dependent

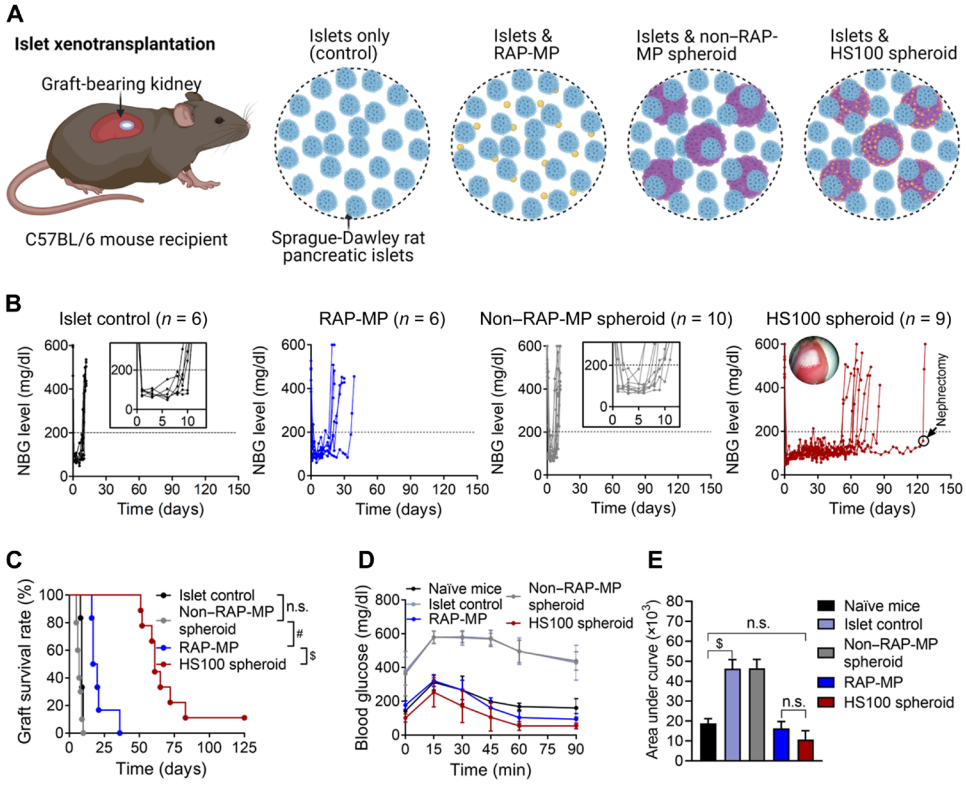

Fig. 4. Locoregional delivery of hybrid spheroids promotes pancreatic rat-to-mouse islet xenograft survival. (**A**) Graphical illustration of the islet xenotransplantation model. STZ-rendered diabetic C57BL/6 mice were transplanted with 400 IEQs of islets only (control) or with RAP-MPs, non–RAP-MP spheroids, or HS100 spheroids under kidney capsules. Twenty spheroids, equivalent to 0.5×10^6 MSCs, were used per transplant. (**B**) NBG levels of recipient mice. (**C**) Kaplan-Meier curves of islet xenograft survival times. (**D**) Intraperitoneal glucose tolerance test (IPGTT) results at 12 days after transplantation and (**E**) area under the curve of IPGTT results ($n = 3$, means ± SDs). The data in (C) and (E) were analyzed using the log-rank (Mantel-Cox) test and one-way analysis of variance (ANOVA), respectively. #$P < 0.001$ and \$$P < 0.0001$. n.s., not significant.

manner. Recipients administered HS10, HS40, HS100, or HS200 spheroids achieved MSTs of 52 days (means ± SD = 59.6 ± 38.5 days), 62 days (means ± SD = 55.2 ± 35.8 days), 61 days (means ± SD = 69.9 ± 22.9 days), and 95.5 days (means ± SD = 75.4 ± 34.9 days), respectively (all P values < 0.0001 versus islet control and non–RAP-MP spheroid groups; Fig. 4, B and C, and fig. S10). Among islet recipients that received localized hybrid spheroids, there were 79% (19 of 24), 17% (4 of 24), and 8% (2 of 24) of grafts remaining functional for ≥50, ≥100, and >125 days, respectively. Long-term graft acceptance (>125 days) was achieved by HS10 spheroid group ($n = 1$) and HS100 spheroid group ($n = 1$) (black circles; Fig. 4B and fig. S10). Notably, levels of RAP in serum in the HS100 spheroid group were almost undetectable at any time.

To assess the immunoprotective role of sustained RAP release, we cotransplanted islets with non–RAP-MP spheroids that had been preconditioned with 100 nM RAP solution for 3 days. We found that islet graft rejection occurred as early (MST = 10 days) as that observed in the islet control and non–RAP-MP spheroid groups (fig. S11, A and C). Moreover, locoregional delivery of hybrid spheroids to islet regions was essential for generating an immunoprotective effect because transplantations of islets and HS100 spheroids under capsules of contralateral kidneys resulted in early islet rejection (MST = 10 days, $P = 0.1842$ versus islet control; figs. S11, B and C). Further, we tested whether spheroids derived from human MSCs had a protective effect on islet xenograft survival. However, cotransplantation of islets and human MSC-derived HS100 spheroids failed to extend islet survival (MST = 9 days, $P = 0.7319$ versus islet control; fig. S12).

Responsiveness of transplanted islets to a glucose spike at 12 days after transplantation was assessed by intraperitoneal glucose tolerance test (IPGTT). Animals in the HS100 spheroid and RAP-MP groups adapted to this glucose elevation in the same manner as nondiabetic (naïve) mice (Fig. 4, D and E). In contrast, blood glucose reductions were delayed in the islet control and non–RAP-MP spheroid groups, indicating islet malfunction at this time.

Locoregionally delivered hybrid spheroids reduce systemic immune activation and favor local immunoregulatory T cell generation

To investigate immune responses, blood, spleen (SPL), draining lymph nodes (DLNs), and grafts were collected at 12 days after transplantation. Serum cytokine levels were determined using a cytometric bead array (CBA) mouse T helper cell 1 (T_H1)/T_H2/T_H17 cytokine kit (Fig. 5A and fig. S13). Results showed significant increases in the serum levels of both inflammatory and anti-inflammatory cytokines after control islet transplantation to the following levels: interleukin-2 (IL-2) (26.0 ± 18.8 pg/ml, $P = 0.006$), IL-4 (28.6 ± 19.1 pg/ml, $P = 0.0037$), IL-6 (27.1 ± 17.9 pg/ml, $P = 0.0038$), IL-10 (32.6 ± 15.8 pg/ml, $P = 0.0022$), IL-17 (36.5 ± 32.3 pg/ml, $P = 0.0266$), IFN-γ (31.0 ± 21.8 pg/ml, $P = 0.013$), and TNF-α (30.6 ± 17.9 pg/ml,

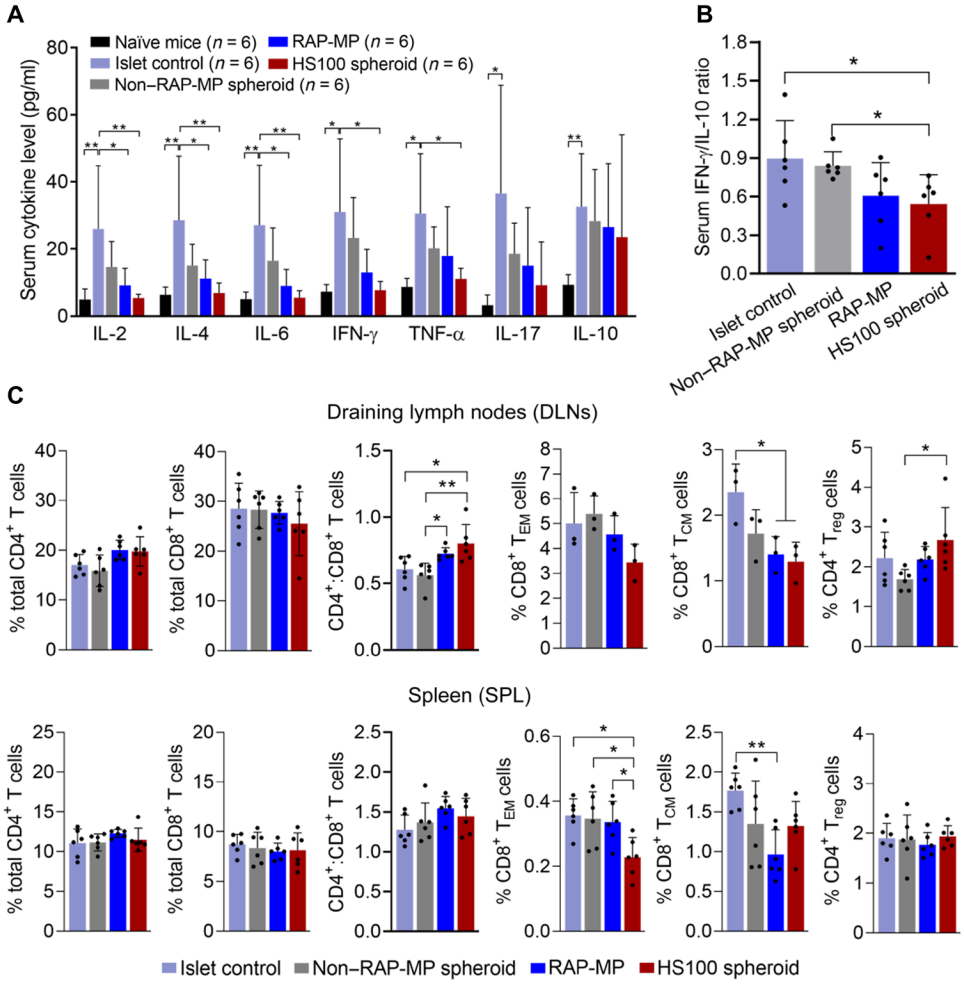

Fig. 5. Locoregional delivery of hybrid spheroids inhibits systemic immune responses to islet transplantation. Serum and lymphoid organs were collected at 12 days after transplantation. (**A**) Serum levels of cytokines ($n = 6$). (**B**) Serum IFN-γ/IL-10 ratios. (**C**) Percentages of T cell populations on total gated cells in DLNs and SPLs ($n = 3$ to 6), as determined by flow cytometry. Gating strategies for regulatory $CD4^+$ $FoxP3^+$ T cells (T_{reg}), effector memory $CD8^+$ $CD44^{high}$ $CD62L^{low}$ T cells (T_{EM}), and central memory $CD8^+$ $CD44^{high}$ $CD62L^{high}$ T cells (T_{CM}) are shown in fig. S13. Data are expressed as the means ± SDs. Data in (A) and (C) were analyzed using one-way ANOVA, and data in (B) and serum IL-10 levels in (A) were analyzed using the unpaired two-tailed *t* test. *$P < 0.05$ and **$P < 0.01$.

$P = 0.0144$) [the P value of IL-10 was determined using the unpaired two-tailed t test and all others by one-way analysis of variance (ANOVA); all P values versus untreated (naïve) mice]. Locoregional delivery of HS100 spheroids significantly decreased the serum levels of IL-2, IL-4, IL-6, IFN-γ, and TNF-α to 5.4 ± 1.1 pg/ml ($P = 0.0074$), 6.9 ± 3.0 pg/ml ($P = 0.0046$), 5.5 ± 2.1 pg/ml ($P = 0.0048$), 7.7 ± 2.6 pg/ml ($P = 0.0153$), and 11.1 ± 3.2 pg/ml ($P = 0.0345$), respectively (all P values versus islet control). Meanwhile, these cytokine levels slightly decreased in the non–RAP-MP spheroid and RAP-MP groups as compared with the islet control group. In addition, no significant change was observed between serum IL-10 levels among the transplanted groups. To determine immune activation statuses, we calculated IFN-γ/IL-10 ratios (a surrogate of T_H1/T_H2 cell ratios in blood) (*27*–*29*). IFN-γ/IL-10 ratios showed the following decreasing trend in the study groups: islet control (0.90 ± 0.29), non–RAP-MP spheroid (0.84 ± 0.11), RAP-MP (0.61 ± 0.26), and HS100 spheroid (0.54 ± 0.23, $P = 0.0411$ versus islet control; unpaired two-tailed t test; Fig. 5B). Overall, these data indicated reduced immune activation upon locoregional delivery of hybrid spheroids.

Next, immune cells were harvested from DLNs and SPLs and subjected to flow cytometry (Fig. 5C and fig. S14). Percentages of immune cell populations were calculated on the basis of total numbers of gated cells. In both lymphoid organs, no significant difference was observed in total $CD4^+$ and $CD8^+$ T cell percentages among the transplanted groups. However, the $CD4^+/CD8^+$ T cell ratio in DLNs was significantly lower in the islet control and non–RAP-MP spheroid groups than in the RAP-MP and HS100 spheroid groups. Notably, HS100 spheroid administration, versus islet control group, sharply reduced the generation of both effector memory $CD8^+CD44^{high}CD62L^{low}$ T cells ($CD8^+$ T_{EM}) (DLNs: 3.44 ± 0.73% versus 5.01 ± 1.24%, $P = 0.2127$; SPL: 0.23 ± 0.06% versus 0.35 ± 0.08%, $P = 0.0144$) and central memory $CD8^+CD44^{high}CD62L^{high}$ T cells ($CD8^+$ T_{CM}) (DLNs: 1.29 ± 0.30% versus 2.35 ± 0.43%, $P = 0.0235$; SPL: 1.32 ± 0.31% versus 1.77 ± 0.22%, $P = 0.1786$). Furthermore, localized HS100 spheroids facilitated the generation of regulatory $CD4^+FoxP3^+$ T cells [$CD4^+$ regulatory T cell (T_{reg})] in DLNs (2.67 ± 0.81% versus 1.68 ± 0.26% in the non–RAP-MP spheroid group, $P = 0.0355$).

Graft-bearing kidneys were also used to evaluate local immune responses at 12 days after transplantation (Fig. 6A). Immune-related gene expression in grafts was analyzed by qRT-PCR. As shown in Fig. 6B, the HS100 spheroid group exhibited significant decreases in *PRF1* and *IFNG* and significant increases in *TGFB1* and *FOXP3* expressions by at least threefold versus the islet control group ($P < 0.05$). In addition, the expressions of *GRMB* and *IL10* tended to decrease and increase, respectively, after HS100 spheroid transplantation. Unexpectedly, *TNF* expression was not significantly altered among the transplanted groups. Besides, we found that the expressions of *TGFB1* and *FOXP3* in the RAP-MP group were lower than in the HS100 spheroid group, whereas other gene expressions were comparable between the two groups.

The histomorphometric characteristics of islet xenografts were assessed by hematoxylin and eosin and multiplex immunohistochemical staining at 12 days after transplantation (Fig. 6C and fig. S15). In the islet control and non–RAP-MP spheroid groups, massive numbers of host cells (especially T cells, blue-stained) infiltrated grafts, and transplanted islets were destroyed and weakly stained brown for insulin. In contrast, host cell recruitment to the grafts containing HS100 spheroids or RAP-MP at this time was much reduced. Although, many intact islets were only observed in the HS100 spheroid group but not the RAP-MP group; in the latter group, many islets were being destroyed, indicating the sign of islet rejection soon after this day (Fig. 6C and fig. S15). The abundance of FoxP3-positive T_{reg} cells (purple-stained) among general infiltrated

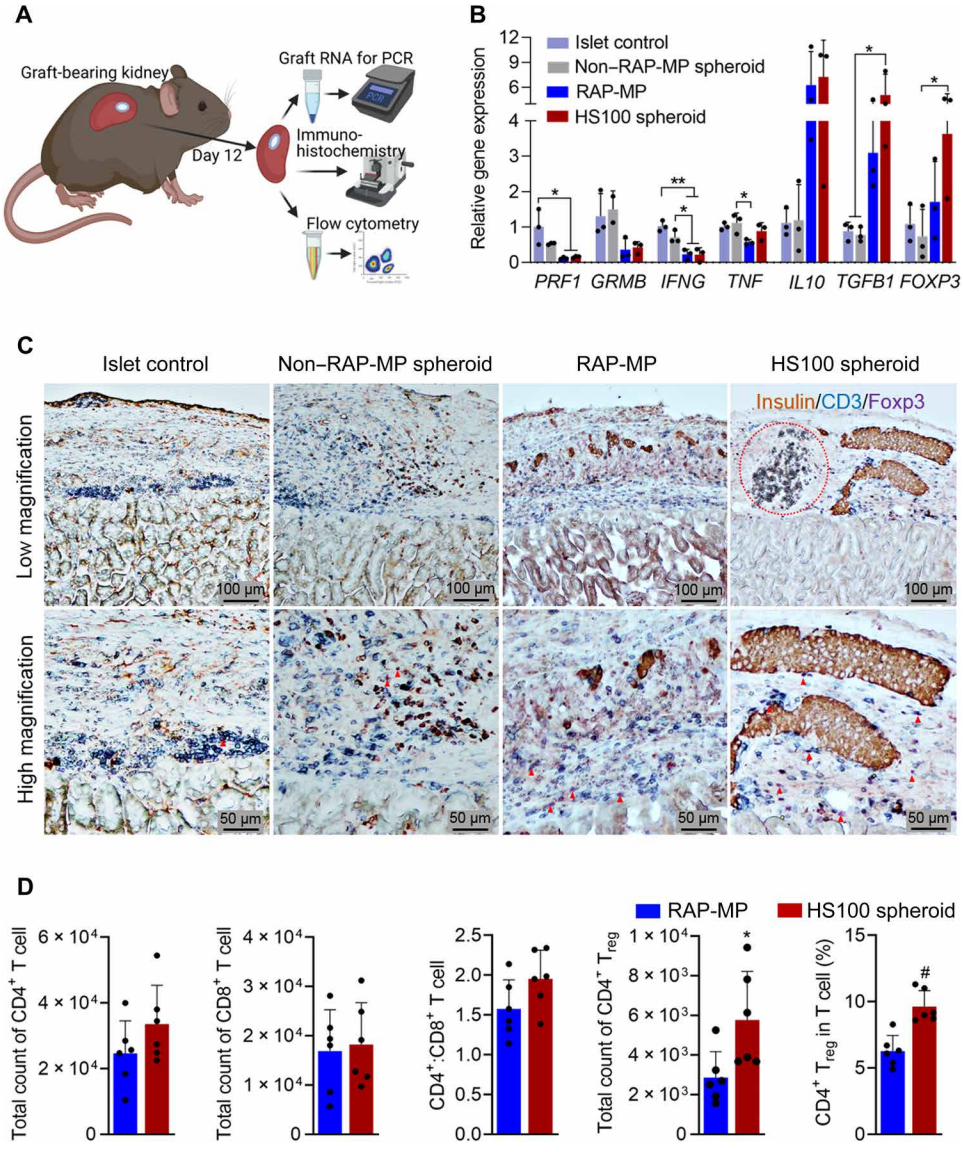

Fig. 6. Locoregionally delivered hybrid spheroids reduce local immune activation and favor T_{reg} cell generation. (**A**) Graphical illustration of islet graft processing for different analysis. (**B**) Relative expressions of genes encoding for perforin (*PRF1*), granzyme B (*GRMB*), IFN-γ (*IFNG*), TNF-α (*TNF*), IL-10 (*IL10*), TGF-β1 (*TGFB1*), and FoxP3 (*FOXP3*) ($n = 3$). (**C**) Representative images of multiplex immunohistochemical graft staining. The red dashed circle indicates a RAP-MP region in HS100 spheroid. Red arrowheads indicate $FoxP3^+$ T_{reg} cells. (**D**) Flow cytometry of T cell populations in the RAP-MP and HS100 spheroid groups ($n = 6$). The data in (B) and (D) are expressed as the means ± SDs and were analyzed using one-way ANOVA and the unpaired two-tailed *t* test, respectively. $^*P < 0.05$, $^{**}P < 0.01$, and $\#P < 0.001$.

T cells was greatest in the HS100 spheroid group. To quantitatively assess immune cell populations, islet grafts in the HS100 spheroid and RAP-MP groups were collected on day 12 after transplantation, dissociated into single cells, and analyzed by flow cytometry (Fig. 6D and fig. S16). We found that the number of $CD4^+$ T cells and the $CD4^+/CD8^+$ T cell ratio were slightly higher in the HS100 spheroid group but that the number of $CD8^+$ T cells was unchanged. Notably, the absolute number and percentage of $CD4^+$ T_{reg} cells in grafts were significantly higher in the HS100 spheroid group than in the RAP-MP group. Together, these results suggested that locoregionally delivered hybrid spheroids reduced systemic immune activation and favored the generation of T_{reg} cells.

Enhanced PD-L1 expression in hybrid spheroids is essential for their immunomodulatory effects

To track the fate of MSCs after transplanting non–RAP-MP or HS100 spheroids with islets, green fluorescent protein (GFP)–expressing MSCs were used to fabricate spheroids. Graft-bearing kidneys were then retrieved to detect GFP signals. As observed, GFP intensities in both groups markedly decreased over time. However, retention time of MSCs in the HS100 spheroid group was significantly improved as compared to non–RAP-MP spheroid group, with the GFP signal intensities on day 10 remained 25.5 ± 16.1% versus 0.7 ± 1.0% (P = 0.019). In addition, on day 20 after transplantation, GFP signals were still detected in the HS100 spheroid group (6.4 ± 3.5%) but not in the non–RAP-MP spheroid group (Fig. 7, A and B).

Next, we tested the gene expression of *PD-L1*, which plays a crucial role in immunomodulation (*30*–*32*), in whole islet xenografts 12 days after transplantation. The expression of *PD-L1* was much higher in the HS100 spheroid group than in the non–RAP-MP spheroid group (2.8 ± 1.4-fold change, P = 0.0411; Fig. 7C). We also examined the effect of PD-L1 on islet xenograft survival. Animals in the HS100 spheroid group were intraperitoneally injected with two doses of anti–PD-L1 antibody solution or an isotype control antibody solution (2.5 mg/kg per dose) at 10 and 20 days after transplantation (Fig. 7D). NBG levels revealed that islet grafts were rejected soon after anti–PD-L1 therapy (MST = 18 days), whereas islet grafts in isotype control antibody group were still functional on day 40 after transplantation (P < 0.01; Fig. 7, E and F).

We hypothesized that PD-L1 expressed by transplanted MSCs in hybrid spheroids might contribute to their immunomodulatory effects in vivo. To examine the surface expression of PD-L1 protein on MSCs in vitro, spheroids were incubated in the presence or absence of a cytokine cocktail containing IFN-γ (20 ng/ml) and TNF-α (10 ng/ml) for 3 days (Fig. 7G). Flow cytometry showed that PD-L1 surface expression was low in a nonstimulating condition but markedly higher after the exposure to the cytokine cocktail. Notably, MSCs from the HS100 spheroid group showed consistently higher PD-L1 levels under both nonstimulating and stimulating conditions with expressional changes of 1.31 ± 0.04-fold and 3.14 ± 0.29-fold, respectively, over non–RAP-MP spheroid group (P values < 0.01). We also examined PD-L1 surface expressions on MSCs after transplantation of non–RAP-MP or HS100 spheroids with islets. To do so, MSCs were labeled with carboxyfluorescein diacetate succinimidyl ester (CFDA-SE) before fabricating spheroids (fig. S17). Grafts were retrieved 7 days after transplantation and subjected to flow cytometry (Fig. 7H and fig. S18). The percentage of the $CFDA\text{-}SE^+$ $PD\text{-}L1^+$ MSC population was found to be higher in grafts containing HS100 spheroids than non–RAP-MP spheroids (94.1 ± 2.6% versus 89.2 ± 3.8%, respectively). HS100 spheroids also exhibited significantly higher surface PD-L1 levels, with ~3-fold increase in the median fluorescence intensity (P = 0.038). To examine the role of PD-L1 expressed by MSCs on islet xenograft survival, MSCs were transfected twice with 50 nM PD-L1 small interfering RNA (siRNA) or 50 nM scrambled siRNA before transplantation (Fig. 7I and fig. S19). Islet grafts in PD-L1 siRNA–transfected group were rejected early as an MST of 22 days (P = 0.0256 versus scrambled siRNA-transfected group; Fig. 7, J and K). These observations showed that enhanced PD-L1 expression on MSCs was responsible for the observed improvement in MSC retention and islet xenograft survival in the HS100 spheroid group.

DISCUSSION

This work was undertaken to devise a means of enhancing the immunomodulatory potency of MSCs by fabricating hybrid spheroids of MSCs with RAP-MPs. The performance of hybrid spheroids was challenged with strong immune responses elicited from the transplantation of xeno-sourced islets in diabetic immunocompetent C57BL/6 mice (*4*). The rationale behind the design of the devised platform was based on the following observations: (i) MSC spheroids achieved better immunomodulatory effects and produce stronger survival signals than 2D-MSCs; (ii) large hybrid spheroids maintained high cell viability in culture; (iii) the uniform distribution of RAP-MP depots in hybrid spheroids enabled better control of cell fate; and (iv) a single localized low-dose RAP-MP containing hybrid spheroids promoted islet xenograft survival, without suboptimal systemic immunosuppression.

The fabrication of hybrid spheroids in our study was motivated by the natural swelling capacity of high molecular weight methylcellulose (viscosity, 4000 cP)–containing medium (*33*, *34*). The concentration of methylcellulose was a critical factor for its applications. Hybrid spheroids were produced from cell-particle suspension in 2 to 3% methylcellulose medium. In particular, after injecting concentrated cell-particle suspension into this methylcellulose medium, spherical droplets form spontaneously, and the methylcellulose then absorbs the water contained in these droplets to rapidly form spheroids. Previously, Kojima *et al.* (*33*) fabricated spheroids containing a small number of cells (1000 cells), which raised no concerns regarding cell viability. However, we here fabricated large spheroids containing 2.5×10^4 MSCs, and these spheroids exhibited high cell viability, which was not obtained when using the hanging drop method. This result emphasizes the role of sufficient nutrients during the preparation process on the maintenance of cell viability. In addition, the devised method enabled adequate control of cell numbers, drug amounts, and their distribution in the hybrid spheroids produced. Notably, most of the spheroid preparation methods reported in the literature are ineffective in terms of the consistency of microparticle incorporation, possibly due to the different densities of cells and microparticles (*35*–*38*). We believe that the hybrid spheroids produced in the present study could serve as a platform for studies on the effects of therapeutic agents on biological cells. Furthermore, it could be feasible for scaling-up the manufacture of hybrid spheroids in methylcellulose with robotic and microfluidic production systems (*39*–*41*).

RAP is one of the most potent drugs in terms of potentiating the immunomodulatory properties of MSCs (*42*). In this study, we found that the colocalization of islets with hybrid spheroids containing

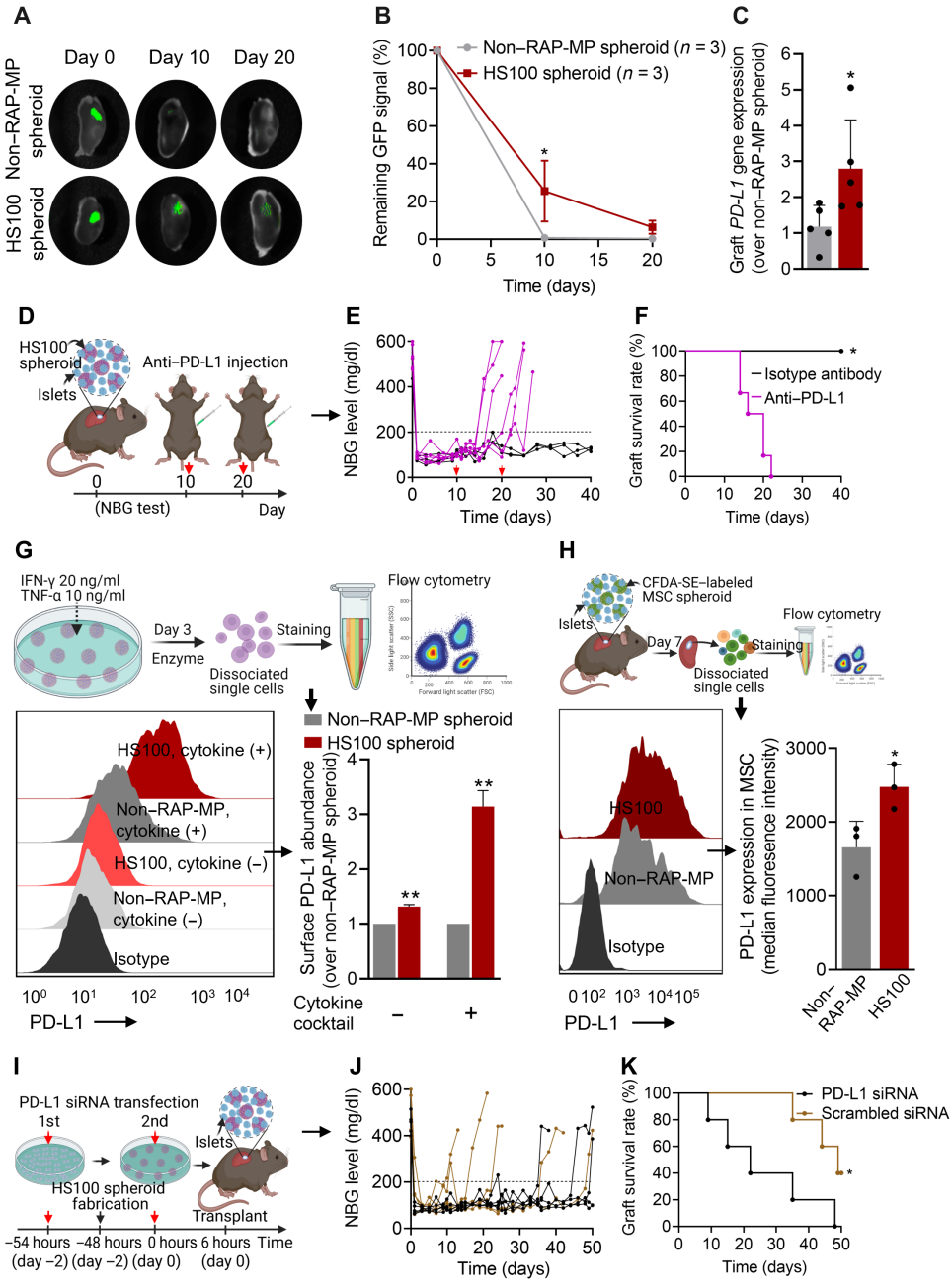

Fig. 7. The essential role played by MSC-mediated PD-L1 on islet xenograft survival. (**A** and **B**) Retention of GFP-expressing MSCs in islet xenografts over time (values are residual GFP intensities; $n = 3$). (**C**) Relative gene expression of *PD-L1* in whole grafts containing islets and non–RAP-MP or HS100 spheroids at 12 days after transplantation ($n = 5$). (**D** to **F**) The effect of anti–PD-L1 antibody treatment (2.5 mg/kg per dose × 2 doses, intraperitoneally delivered on days 10 and 20 after transplantation; $n = 6$) on mice cotransplanted with islets and HS100 spheroids. (D) Graphical illustration of the experimental design, (E) NBG test results, and (F) Kaplan-Meier curves for islet xenograft survival times. Transplanted mice treated with isotype control antibody served as controls ($n = 3$). (**G** and **H**) In vitro and in vivo PD-L1 protein expressions on MSCs in non–RAP-MP and HS100 spheroids, as determined by flow cytometry. (G) Spheroids were treated with or without a cytokine cocktail for 3 days before the assessment ($n = 2$ per group). (H) MSCs were labeled with CFDA-SE before fabricating spheroids. Grafts were retrieved at 7 days after transplantation ($n = 3$). MSCs were considered to express PD-L1 if double-positive for CFDA-SE and PD-L1. (**I** to **K**) Effect of MSC-mediated PD-L1 on islet xenograft survival. (I) Graphical illustration of the experimental design. MSCs were transfected twice with 50 nM PD-L1 siRNA or 50 nM scrambled siRNA before transplantation, (J) NBG test results, and (K) Kaplan-Meier curves of islet xenograft survival times ($n = 5$). Data are expressed as the means ± SDs. Data in (B) were analyzed using two-way ANOVA, in (C), (G), and (H) using the unpaired two-tailed *t* test, and in (F) and (K) using the log-rank (Mantel-Cox) test.

MSCs and RAP-MPs under the kidney capsules of diabetic mice effectively prolonged islet survival time. In addition, the sustained release of RAP was essential for long-lasting impact on MSC performance. We did not observe any improvement in islet graft survival time when islets were cotransplanted with non–RAP-MP spheroids preconditioned with 100 nM RAP solution for 3 days. The devised approach prevents systemic exposure and subsequent adverse effects of immunosuppressant by minimizing the total dose of RAP administered. Furthermore, we observed a synergistic effect between MSCs and RAP over a wide range of RAP doses (200 to 4000 ng per mouse). Previously, studies reported the effectiveness of 2D-MSCs (1×10^6 cells per transplant) and daily systemic RAP (0.1 mg/kg per day, 7 to 9 days) on allogeneic islet survival (*12*, *13*). The total doses of RAP administered in these studies were around 15 to 20 μg per mouse, which was 4 to 80 times higher than those used in our current study. In addition, while daily drug injections are inconvenient and result in variable drug biodistributions, we demonstrated that the performance of our designed hybrid spheroids was local and not dependent on the systemic presence of RAP. By that, the administered doses of drugs can be optimized and fixed, regardless the recipient body weight (*43*). Given the adverse effects of immunosuppressive drugs, our approach on the localization of hybrid spheroids offers an efficient means of inducing immunotolerance in clinical transplantation field.

The mechanisms by which RAP modulates MSC immunomodulatory functions remain unclear. Wang *et al.* (*15*) discovered that short-term exposure to RAP (4 hours) enhanced the inhibitory effect of human MSCs on T cell proliferation in vitro by transiently increasing COX-2 and PGE-2 secretions, although the in vivo relevance of this observation needs to be confirmed. Meanwhile, other studies revealed that human MSCs treated with RAP for 24 to 48 hours exhibited increased expressions of *IL10*, *TGFB1*, *IDO1*, *INOS*, and *COX-2* and established that enhanced autophagy was responsible (*44*, *45*). In a mouse model, injection of RAP-preconditioned MSCs effectively ameliorated the clinical severities of acute graft-versus-host disease (*44*). In the current study, we investigated 14 crucial immune-related genes in MSCs, which are well reported in the literature (*11*, *15*, *46*–*49*). Among these genes, *CD86*, *MHC-I*, and *MHC-II* are related to the immunogenicity of MSCs, whereas *PD-L1*, *TGFB1*, *IL1RN*, *IDO1*, *INOS*, *HO-1*, *COX-1/2*, and *IL4/6/10* are related to anti-inflammatory and immunomodulatory properties of MSCs. The results obtained confirmed that RAP enhanced the gene expressions of *IL10*, *TGFB1*, and *COX-2* but not those of *IDO1* and *INOS*. These results suggest that *IDO1* and *INOS* might not be the main factors responsible for the performance of hybrid spheroids in our disease model. In addition, we found that RAP induced stable increases in the gene expressions of *PD-L1*, *MHC-I*, and *IL6*, which has not been reported previously. Among the immunomodulatory molecules, MSC-derived PD-L1 plays a master role in the modulation of immune responses (*31*, *46*). To the best of our knowledge, this is the first report of PD-L1 expression in adipose tissue–derived MSCs (*46*). The engagement of PD-1 on activated T cells with PD-L1 interrupts the activation cascade in these cells, which leads to a change in effector cell state and the generation of T_{reg} cells (*50*). MSCs have been found to inhibit T cell proliferation via both cell surface–bound PD-L1 and soluble PD-L1 (*51*, *52*). To demonstrate the role of PD-L1 on islet xenograft survival, we injected islet recipients intraperitoneally with anti–PD-L1 antibody and inhibited the synthesis of PD-L1 in MSCs by siRNA transfection. Anti–PD-L1 antibody injection blocked PD-L1 expression in many cell types, including T_{reg} cells, antigen-presenting cells, and MSCs, and thus compromised their protective roles on islet survival. siRNA-mediated PD-L1 silencing in hybrid spheroids was also found to effectively shorten islet survival, despite the transient nature of its effect. These observations suggest that PD-L1 siRNA–transfected hybrid spheroids might be more sensitive to T cell attack during the first days following transplantation (*53*) and that enhanced PD-L1 expression in hybrid spheroids was essential to protect transplanted islets from early rejection. Short-term silencing of genes in MSCs with siRNAs has been demonstrated to have long-term effects after cell transplantation (*54*). Xu *et al.* (*55*) showed that subcutaneous injection of RUNX2 siRNA–transfected MSCs effectively promoted their chondrogenic differentiation by inhibiting RUNX2-mediated hypertrophy. In another study, MSCs were transfected with the plasmid encoding for siRNA targeting Fas receptor and miR-375 genes, and codelivery of these MSCs with pancreatic islets significantly improved islet survival and function (*56*).

Cheng *et al.* (*12*) demonstrated that treatment with MSCs derived from human induced pluripotent stem cells plus a short-course (9 days) systemic injections of RAP effectively developed islet allograft tolerance. Nevertheless, our attempts to transplant hybrid spheroids prepared using human MSCs and RAP-MPs failed to protect islet xenograft from early rejection. Even, we found that the MST of this human MSC-derived hybrid spheroid group was shorter than that of RAP-MP group. These data raised some issues regarding the immunogenicity of human MSCs in mouse recipients. For example, the structural similarity between human and mouse PD-L1 is 77% whereas that between human and mouse PD-1 is 64%. Mouse PD-1 can interact with human PD-L1 in vitro (*57*, *58*). However, it has not been established whether this interspecies interaction has therapeutic benefits in vivo. In addition, recently published data show that mouse and human PD-L1 molecules are structurally similar but they have different druggability profiles (*59*).

More recently, Coronel *et al.* (*60*) demonstrated that locally delivered PD-L1–presenting poly(ethylene glycol) microgels in combination with daily injections of RAP (0.2 mg/kg per day, i.p., for 15 days) led to the development of islet allograft tolerance in murine epididymal fat pads. Encouraged by this finding and the results of our current study, we suggest that further studies be conducted to investigate the effect of the stable overexpression of PD-L1 from MSCs on the induction of tolerance to clinically relevant xeno-sourced islets. Notably, MSCs express high levels of PD-L1 as encountering immune cells, but existing inflammatory cytokines may have detrimental effects on MSC viability and, thus, reduce the duration of immunomodulation by MSCs. Pre- and stable overexpression of PD-L1 would be essential to maintain MSC viability after transplantation. Although we placed emphasis on PD-L1 signaling, the roles of other immune checkpoints and paracrine mediators on the performance of MSCs are also important (*61*, *62*). These molecules may act synergistically to inhibit the activity of effector T cells and favor the generation of T_{reg} cells (*3*, *11*). In addition, the direct effect of RAP released from the hybrid spheroids on immune cells should be counted. This study indicates that RAP enhanced MSC potency in hybrid spheroids, at least in terms of modulating PD-L1 expression, and we believe that this mechanism was largely responsible for improved islet xeno-transplantation outcomes observed. Our future studies will further optimize hybrid

spheroids by coincorporation of different therapeutic agents (*63*). These agents would be used to target on MSCs or other immune cells (T cell, macrophages, and dendritic cells), and therefore, the immunomodulatory effect of hybrid spheroids would be durable in establishing islet graft tolerance. We envision that proximal localization of hybrid spheroids and pancreatic islets would be efficiently used in extrahepatic transplantation sites, such as subcutaneous space, anterior chamber of eyes, omentum, and gastric submucosa, which have shown great potentials as revealed in many recent clinical trials (*64*). Especially, the development of implantable dual-reservoir encapsulation devices is highly encouraged because it enables a precise localization of individual therapeutic cells and drug depots for better control of cell fate (*65*). It is also possible to recharge protective cell drug depots to islet grafts for maintaining immunomodulatory effects in an extended period of time. Last, our current study provides a flexible means of using MSCs efficiently in the transplantation field and for the treatments of various inflammatory conditions.

MATERIALS AND METHODS

Illustrative images were created with BioRender.com. All experiments on animals were performed in accordance with national guidelines and approved by the Institutional Animal Care and Use Committee of Yeungnam University (Gyeongsan-si, Gyeongbuk-do, Republic of Korea).

Preparation and characterization of RAP-MPs

RAP was encapsulated in PLGA microparticles using an oil-in-water emulsification method, as previously described (*66*–*68*). Briefly, 76 mg of PLGA (Resomer RG504 H; Sigma-Aldrich, Saint Louis, MO, USA) and 4 mg of RAP (LC Laboratories, Woburn, MA, USA) were solubilized in 1 ml of dichloromethane (Junsei Chemical Co. Ltd., Tokyo, Japan). Next, emulsion was made by emulsifying the organic phase in 5 ml of 1% polyvinyl alcohol (PVA) solution (Sigma-Aldrich, Saint Louis, MO, USA) at 21,000 rpm for 4 min. The emulsion produced was stabilized in excess PVA solution for 4 hours, and RAP-MPs were collected after 5 cycles of centrifugation and washing. Last, RAP-MPs were lyophilized to a dry powder. The size of RAP-MPs was determined by SEM (S-4100; Hitachi, Tokyo, Japan), and the chemical properties of RAP was tested by Fourier transform infrared spectroscopy (Nicolet Nexus 670 FTIR Spectrometer; Thermo Fisher Scientific, Waltham, MA, USA) (*66*, *69*).

The RAP loading capacity of RAP-MPs was quantified by HPLC analysis. RAP was extracted from RAP-MPs using acetonitrile (ACN; Junsei Chemical Co. Ltd., Tokyo, Japan), which was then filtered through a 0.22-μm membrane. Chromatographic parameters were as follows: Inertsil column (4.6 mm by 150 mm, 5 μm; GL Sciences, Tokyo, Japan), isocratic elution with ACN:water (85:15) at 1 ml/min, peak detection at 280 nm, and column temperature 60°C. In vitro release of RAP-MPs was evaluated in phosphate-buffered saline (PBS) (pH 7.4) containing 1% Tween 20. RAP-MP suspensions were shaken in an incubator (SI-64, 150; Hanyang Scientific Equipment Co. Ltd., Seoul, Republic of Korea) and maintained at 37°C and 150 rpm, and, at predetermined times, supernatants were withdrawn to quantify RAP levels.

Isolation and characterization of mouse adipose–derived MSCs

MSCs were isolated from C57BL/6 mice (male, 8 to 10 weeks old; Samtako Bio Korea, Osan-si, Gyeonggi-do, Republic of Korea), as previously described with some modifications (*70*, *71*). Briefly, the mice were euthanized and immersed in 70% ethanol. Next, subcutaneous adipose tissue was exposed, collected, chopped, and digested with 0.1% collagenase type P solution (Sigma-Aldrich, Saint Louis, MO, USA) for 30 min at 37°C and 80 rpm. MEM-α growth medium containing 10% fetal bovine serum (FBS) and 1% penicillin-streptomycin antibiotics 100× (Thermo Fisher Scientific, Waltham, MA, USA) was then added to neutralize enzyme activity, and cells were pelletized by centrifugation at 400*g* for 5 min. After redispersing in MEM-α growth medium, the samples were passed through a 40-μm cell strainer to remove residual fibers and fat cells. Filtrates were cultured at 37°C, and on the next day, adherent MSCs were rinsed carefully with PBS to remove debris and unattached cells. Culture was continued (with frequent medium changes) to 80 to 90% confluence. MSCs from passages 3 to 6 were used in the experiments. In some experiments, GFP-expressing MSCs were isolated from C57BL/6 transgenic mice strain expressing GFP (male, 8 to 10 weeks old; The Jackson Laboratory, Bar Harbor, ME, USA). Human adipose tissue–derived MSCs [ASC(ST002); Epibiotech, Incheon Metropolitan City, Republic of Korea] were also used. Isolated MSCs were characterized by evaluating the expressions of cell surface markers ($CD29^+$, $CD44^+$, $CD90^+$, $Sca\text{-}1^+$, $CD11b^-$, $CD34^-$, and $CD45^-$) and by their capacity to differentiate into three lineages (osteoblasts, chondrocytes, and adipocytes), as previously described (*23*).

Fabrication of hybrid spheroids

Hybrid spheroids were fabricated using a free water-absorbable viscous polymer-based method, as previously described (*33*). The polymer solution was composed of 2% methylcellulose (Sigma-Aldrich, Saint Louis, MO, USA) in MEM-α growth medium. To construct one spheroid, 2.5×10^4 MSCs were thoroughly mixed with RAP-MPs in MEM-α growth medium to produce 2 μl of a cell-particle suspension, and this suspension was then slowly injected into methylcellulose solution and incubated for 2 hours at 37°C to promote spontaneous cell-particle aggregation. After adding MEM-α medium to lower the viscosity of methylcellulose, the spheroids produced were retrieved using a pipette, washed twice with MEM-α medium, and cultured on a nonadherent petri dish (100 mm by 15 mm; SPL Life Sciences, Pocheon-si, Gyeonggi-do, Republic of Korea). Hybrid spheroids containing different amounts of RAP-MPs (10, 40, 100, and 200 ng of RAP per spheroid) were fabricated; these are referred to as HS10, HS40, HS100, and HS200, respectively. MSC spheroids not containing RAP-MPs are referred to as non–RAP-MP spheroids. To visualize RAP-MPs in hybrid spheroids, they were labeled with 0.1% coumarin-6 (Sigma-Aldrich, Saint Louis, MO, USA).

Morphology and size distribution of spheroids

The morphologies of non–RAP-MP and hybrid spheroids were observed under an optical microscope (Eclipse Ti; Nikon Instruments Inc., Melville, NY, USA). At least 30 spheroids were randomly measured, and size distributions were determined using NIS-Elements BR software version 4.20.00 (Eclipse Ti; Nikon Instruments Inc., Melville, NY, USA).

Microsphere distribution in hybrid spheroids

The distribution of microparticles in hybrid spheroids was first examined by CLSM (Nikon A1si, Nikon Instruments Inc., Melville,

NY, USA). Briefly, on the third day of culture, hybrid spheroids were collected, rinsed with PBS, and fixed in 4% paraformaldehyde (PFA; Sigma-Aldrich, Saint Louis, MO, USA). Cell nuclei were then counterstained with Hoechst 33342 solution (1:1000; Thermo Fisher Scientific, Waltham, MA, USA) for 20 min at room temperature (R.T.). Samples were then scanned, and 3D images of hybrid spheroids were reconstructed using Nis-Element software.

Spheroids were also examined using SEM (S-4100; Hitachi, Tokyo, Japan), as previously described (*72*). Briefly, samples were fixed in 4% glutaraldehyde solution for 60 min and then sequentially coated with 1% osmium tetroxide (OsO_4), 3% carbohydrazide, and 1% OsO_4 for 15 min each. All materials were purchased from Tokyo Chemical Industry Co. (Tokyo, Japan). Dried spheroids were halved using a sharp blade and spray-coated with a thin platinum layer before observation.

Cell viability assessment

A live/dead staining test was used to evaluate cell viability. Briefly, spheroids were collected, incubated in MEM-α medium containing 0.67 μM acridine orange and 75 μM propidium iodide (PI) (Sigma-Aldrich, Saint Louis, MO, USA) for 30 min at R.T., and visualized using a fluorescence microscope (Eclipse Ti; Nikon Instruments Inc., Melville, NY, USA). In addition, cell viability was quantitatively measured using the PI/fluorescein isothiocyanate–annexin V kit (BioLegend, San Diego, CA, USA). Before staining, spheroids were rinsed with PBS and dissociated into single cells using trypsin. The staining procedure was obtained from manufacturer's instructions. The stained samples were analyzed using flow cytometry (FACSCanto II; BD Biosciences, San Jose, CA, USA).

The apoptotic statuses of cells in spheroids were further assessed by Western blot, as previously described (*73*). Briefly, spheroids were rinsed with PBS, minced into single cells, and lysed with Mammalian Protein Extraction Buffer (MPER; Thermo Fisher Scientific, Waltham, MA, USA). Total proteins (30 to 40 μg) were run on 12% SDS–polyacrylamide gel electrophoresis gels and transferred to polyvinylidene difluoride membranes (Immobilon-P; Merck Millipore, Burlington, MA, USA). Membranes were treated with 5% bovine serum albumin (BSA; Thermo Fisher Scientific, Waltham, MA, USA) in tris-buffered saline (with 0.05% Tween 20) for 1 hour at R.T. and incubated with rabbit anti-BAX (B-cell lymphoma-2 associated X) antibody (1:1000; Cell Signaling Technology, Danvers, MA, USA) or rabbit anti–glyceraldehyde-3-phosphate dehydrogenase (GAPDH) antibody (1:1000; Cell Signaling Technology, Danvers, MA, USA) at 4°C overnight. After rinsing, membranes were incubated with anti-rabbit immunoglobulin G (IgG)–horseradish peroxidase (HRP; 1:5000; Santa Cruz Biotechnology, Santa Cruz, CA, USA) for 1 hour at R.T. Last, the signals were developed with SuperSignal West Pico Chemiluminescent Substrate solution (Thermo Fisher Scientific, Waltham, MA, USA). Spot densities were observed using a Fujifilm LAS-4000 mini system (Fujifilm, Tokyo, Japan).

In addition, caspase 3/7 activity was assessed using a Caspase-Glo 3/7 assay kit (Promega, Madison, WI, USA). Briefly, 2D-MSCs or spheroids were rinsed with PBS and lysed with the MPER lysis buffer. Cell lysates were mixed with Caspase-Glo 3/7 Substrate solution at equal volumes in a white-walled 96-well plate (Corning, Oneonta, NY, USA). After incubation for 2 hours, luminescence of resulting solution was measured. The data were normalized by respective double-stranded DNA levels, measured using a Picogreen assay (Thermo Fisher Scientific, Waltham, MA, USA).

Liquid chromatography–tandem mass spectrometry

At predetermined times, one to three hybrid spheroids were taken in microtubes and rinsed with PBS. RAP was extracted using 0.1 to 1.0 ml of ACN and probe sonication. Samples were then diluted and passed through a 0.22-μm membrane. FK506 (Hanmi Pharma, Seoul, Republic of Korea) was used as an internal standard to compensate for sample matrix effects. Chromatography was carried out on an Agilent 1260 Infinity HPLC (Agilent Technologies, Santa Clara, CA, USA), equipped with an Atlantis dC18 column (2.1 mm by 150 mm, 3 μm; Water Corporation, MA, USA). Gradient elution was performed using ACN and 2 mM ammonium acetate buffer and the following program 0 to 2.5 min: 90% ACN, 2.5 to 10.5 min: 5% ACN, and 10.5 to 16.0 min: 90% ACN, at a flow rate of 250 μl/min and a column temperature of 60°C. MS/MS was performed using an API-400 triple quadrupole unit (AB SCIEX, Framingham, MA, USA) in positive ion mode, and detection was performed by Multiple Reaction Monitoring using the ion transitions of mass/charge ratio 931.8 to 864.6 for RAP and 821.58 to 768.5 for FK506.

Cytokine treatment

To investigate the response of spheroids to inflammatory conditions, they were treated with a cytokine cocktail containing TNF-α (biological activity > 1.0×10^7 U/mg; catalog no. NBP2-35185; Novus Biologicals LLC, CO, USA) and IFN-γ (biological activity 1 to 4×10^6 U/mg; catalog no. 575306; BioLegend, San Diego, CA, USA) at 10 and 20 ng/ml, respectively. At predetermined times, spheroids were retrieved, washed twice with PBS, and processed for qRT-PCR or flow cytometry.

Isolation of rat pancreatic islets

Sprague-Dawley rats (male, 8 to 10 week of age; Samtako Bio Korea, Osan-si, Gyeonggi-do, Republic of Korea) were used as pancreatic islet donors. Briefly, rats were euthanized by cervical dislocation, pancreases were exposed, and 0.08% collagenase type P solution (Sigma-Aldrich, Saint Louis, MO, USA) was injected via the hepatic bile duct. Pancreases were then incubated for 18 min at 37°C. Pancreatic islets were isolated from exocrine cells by using a Histopaque-1077 solution (Sigma-Aldrich, Saint Louis, MO, USA) and cultured in RPMI 1640 growth medium (Mediatech, Manassas, VA, USA) containing 10% FBS and 1% penicillin-streptomycin antibiotics 100× (Thermo Fisher Scientific, Waltham, MA, USA) for 3 days to recover functionality before transplantation (*74*).

GSIS assay

GSIS assay was performed to assess the effect of spheroids on the secretion of insulin by pancreatic islets in vitro. Briefly, 100 IEQs of islets and five spheroids were mixed in 200 μl of RPMI 1640 growth medium, which was then seeded into the 96-well plate precoated with anti-adherence rinsing solution (STEMCELL Technologies, Vancouver, Canada). The cell mixtures were cultured at 37°C for 24 hours. Next, the cell mixtures were collected into microtubes, washed thrice with low-glucose (2.8 mM) solution in Kreb-Ringer bicarbonate buffer, and were preconditioned with the same solution at 37°C for 1 hour. Thereafter, the samples were sequentially incubated in 0.2 ml of fresh solutions containing low glucose, high glucose (16.7 mM), and low glucose at 37°C for 1.5 hours each. The cell supernatant was collected, respectively. The insulin level in the cell supernatant was measured using an Insulin ELISA (enzyme-linked immunosorbent assay) kit (EZRMI-13 K; Merck Millipore,

Darmstadt, Germany). The insulin level was expressed as pg/IEQ/hour. The SI value was calculated by dividing insulin level in high-glucose treatment to that in first low-glucose treatment.

Cell transplantation in C57BL/6 mice

Diabetic C57BL/6 mice (male, 7 to 8 weeks old; Samtako Bio Korea, Osan-si, Gyeonggi-do, Republic of Korea) induced by injecting STZ (200 mg/kg; intraperitoneal route; Sigma-Aldrich, Saint Louis, MO, USA) were used as islet recipients. NBG levels were periodically obtained from venous tail blood to confirm diabetic conditions (NBG $\geq$ 350 mg/dl for two consecutive days). For transplantation, mice were sedated with ketamine/xylazine, kidneys were exposed to create space beneath capsules, and a cell preparation containing 400 IEQs of islets with or without 20 spheroids (equivalent to 0.5×10^6 MSCs) in a PE (polyethylene) tubing (Thermo Fisher Scientific, Waltham, MA, USA) was injected into subcapsular spaces. In the RAP-MP group, islets and RAP-MPs were loaded in separate transplant tubing and sequentially injected. If NBG values were > 200 mg/dl for two consecutive days, then grafts were considered rejected. IPGTT was also carried out to assess the kinetic responses of insulin secretion by transplanted islets to glucose challenge. Briefly, at 12 days after transplantation, mice were kept fasting for 6 hours. Then, mice were injected with a glucose solution (2.0 g/kg) via intraperitoneal route. Glucose levels in blood were recorded at 0-, 15-, 30-, 45-, 60-, and 90-min after injection. Naïve mice with same ages were also used for the comparison.

Quantitative reverse transcription polymerase chain reaction

For the in vitro study, spheroids were collected, rinsed with PBS, and lysed with TRIzol (Thermo Fisher Scientific, Waltham, MA, USA). Chloroform was added, and mRNA in top aqueous layer was separated and purified by serial precipitation using isopropanol and ethanol. For the in vivo study, mRNA was extracted from islet grafts using the ReliaPrep RNA Tissue Miniprep kit (Promega, Madison, WI, USA). cDNA was synthesized using the GoScript Reverse Transcription Kit (Promega, Madison, WI, USA). Then, the SYBR Green Kit (Thermo Fisher Scientific, Waltham, MA, USA) was used for PCR amplification using suitable pairs of primers (see table S1). Target mRNA relative expressions were determined using the comparative threshold (Ct) method; *GAPDH* and 18*S rRNA* were used as housekeeping genes. cDNA synthesis and PCR amplification were performed using a TGradient thermocycler (Biometra, Germany) and a Roche Lightcycler 2.0 (Thermo Fisher Scientific, Waltham, MA, USA), respectively.

Quantification of serum cytokines

Whole blood was taken from beating hearts of recipients by cardiac puncture and left to clot at R.T. for 15 to 30 min. Serum was isolated by centrifuging blood for 10 min at 2000*g* and 4°C. Samples were then stored at −80°C until required. The CBA mouse $T_H1/T_H2/T_H17$ cytokine kit (Thermo Fisher Scientific, Waltham, MA, USA) was used to determine serum cytokine levels. The data were analyzed using FlowJo software version 7.6.2 (BD Biosciences, San Jose, CA, USA).

Flow cytometry

The expressions of protein markers of MSCs and immune cells were determined by fluorescence-activated cell sorting (FACS). Typically, samples were dissociated into single cells by combination of mechanical force, collagenase D (Roche Diagnostics GmbH, Mannheim, Germany) and/or TrypLE Express solution (Thermo Fisher Scientific, Waltham, MA, USA), and rinsed twice with staining buffer (0.3% BSA in PBS). Cells were stained with specific fluorophore-conjugated antibodies (see table S2) for 30 min on ice. After washing, the cells were fixed with 4% PFA solution (Sigma-Aldrich, Saint Louis, MO, USA). The analysis was performed using a FACSCalibur system (BD Biosciences, San Jose, CA, USA). Intracellular antigens were stained according to the manufacturer's instructions (BD Biosciences). Respective isotype control antibodies were used to compensate for nonspecific IgG binding to cell surfaces. Fluorescence minus one samples were also included. Data were processed using FlowJo software version 7.6.2 (BD Biosciences).

Histological study

Graft-bearing kidneys were retrieved to assess histomorphometries at 12 days after transplantation. Samples were fixed in 4% PFA solution (Sigma-Aldrich, Saint Louis, MO, USA) for 1 to 2 days, immersed in 30% sucrose solution (Alfa Aesar, Ward Hill, MA, USA) for 3 days, and sectioned at 10 μm using a freezing microtome (HM450; Thermo Fisher Scientific, Waltham, MA, USA). After mounting the sections on histological slides, epitope retrieval was performed using citrate buffer solution (pH 6.0; 0.05% Tween 20) for 30 min at 98°C in a water bath, and endogenous peroxidase activity was quenched by treating sections with 3% hydroxyperoxide for 15 min. Circles were made around regions of interest using a hydrophobic pen. Triple immunostaining was used to simultaneously stain islets and T cells in grafts, according to instructions issued by Vector Laboratories (Burlingame, CA, USA). Before each antigen staining, nonspecific binding was prevented by treating sections with PBS containing 0.3% Triton X-100 (Sigma-Aldrich, Saint Louis, MO, USA), 2% BSA, and 10% normal goat serum (Vector Laboratories, Burlingame, CA, USA) for 1 hour at R.T. and subsequently with Avidin and Biotin solutions (Vector Laboratories, Burlingame, CA, USA) for 15 min each. Samples were then treated with primary antibody against insulin (1:300; Proteintech, Suite 300 Rosemont, IL, USA), CD3 (1:300; Novus Biologicals LLC, CO, USA), or FoxP3 (1:200; BioLegend, San Diego, CA, USA) at 4°C overnight. After rinsing, samples were stained with biotinylated secondary antibody for 1 hour at R.T. and then with HRP-labeling ABC kit working solution for 30 min at R.T. The signals were developed by incubating sections with ImmPACT DAB (brown) substrate, ImmPACT VIP (purple) substrate, or ImmPACT SG (gray blue) substrate solutions (all from Vector Laboratories) for 2 to 15 min at R.T. Following rinsing and drying steps, sections were fixed with VectorMount Permanent Mounting Medium (Vector Laboratories, Burlingame, CA, USA) and imaged using an optical microscope.

MSC retention in islet grafts

GFP-expressing MSCs were used to assess the retention times of MSCs in islet grafts. Briefly, GFP-MSC–derived spheroids were cotransplanted with islets into subcapsular spaces. Graft-bearing kidneys were collected at 1 hour (day 0) and 10 and 20 days after transplantation. After fixing in 4% PFA solution, samples were imaged in the GFP channel of a Fluorescence-labeled Organism Bioimaging instrument (NeoScience, Suwon, Republic of Korea). Percentages of remaining MSCs were calculated with respect to fluorescence intensities observed at 1 hour (day 0) after transplantation.

In vivo tracking of MSCs

MSCs were stably labeled with CFDA-SE (Thermo Fisher Scientific, Waltham, MA, USA) for in vivo tracking. Briefly, 1×10^6 MSCs were rinsed twice and incubated in 1 ml of PBS containing 20 μM CFDA-SE for 15 min at 37°C. Cell suspensions were mixed using a pipette every 3 min to ensure uniform reaction. Unreacted reagent was then neutralized with 0.5 ml of MEM-α growth medium, and labeled MSCs were rinsed twice before determining labeling efficiencies by flow cytometry.

Anti–PD-L1 antibody injection

To study the role of PD-L1 on islet xenograft survival, islet recipients were given two doses of 100 μl of PBS containing anti-mouse monoclonal anti–PD-L1 antibody (BioXCell, West Lebanon, NH, USA) or IgG2b isotype control (BioLegend, San Diego, CA, USA) at 2.5 mg/kg via intraperitoneal route on days 10 and 20 after transplantation.

siRNA-mediated silencing of PD-L1 in MSCs

MSCs (1.5×10^5) were cultured on a cell culture plate (60 mm by 15 mm; Corning, Oneonta, NY, USA) for 24 hours before transfection. Next day, MSCs were incubated with 2 ml of MEM-α medium containing 50 nM PD-L1 siRNA (No60533-1; Bioneer, Daejeon, Republic of Korea) and Lipofectamine RNAiMAX Transfection reagent (Thermo Fisher Scientific, Waltham, MA, USA) for 6 hours at 37°C. Cells were then rinsed, trypsinized, and used to fabricate hybrid spheroids with RAP-MPs. To increase durations of gene silencing, hybrid spheroids were incubated with the transfection complex for 6 hours before being transplanted with islets. Transfection efficiencies and gene silencing durations were determined by qRT-PCR.

Statistical analysis

GraphPad Prism version 8.4.2 (GraphPad Software Inc., La Jolla, CA, USA) was used to draw graphs and for the statistical analysis. Graft survival times were analyzed using the log-rank (Mantel-Cox) test. One-way ANOVA was used to compare the data of ≥3 groups, whereas the unpaired two-tailed *t* test was used to compare the data of two groups. *P* values of <0.05 were considered statistically significant.

SUPPLEMENTARY MATERIALS

Supplementary material for this article is available at https://science.org/doi/10.1126/sciadv.abn8614

View/request a protocol for this paper from *Bio-protocol*.

REFERENCES AND NOTES

1. J. C. Gea-Banacloche, in *Principles of Molecular Medicine*, M. S. Runge, C. Patterson, Eds. (Humana Press, 2006), pp. 893–904.
2. C. McDonald-Hyman, L. A. Turka, B. R. Blazar, Advances and challenges in immunotherapy for solid organ and hematopoietic stem cell transplantation. *Sci. Transl. Med.* **7**, 280rv2 (2015).
3. U. Kaundal, U. Bagai, A. Rakha, Immunomodulatory plasticity of mesenchymal stem cells: A potential key to successful solid organ transplantation. *J. Transl. Med.* **16**, 31 (2018).
4. G.-B. Im, S. H. Bhang, Recent research trend in cell and drug delivery system for type 1 diabetes treatment. *J. Pharm. Investig.* **48**, 175–185 (2018).
5. S.-B. Yong, J. Y. Chung, Y. Song, Y.-H. Kim, Recent challenges and advances in genetically-engineered cell therapy. *J. Pharm. Investig.* **48**, 199–208 (2018).
6. P. Saeedi, R. Halabian, A. A. Imani Fooladi, A revealing review of mesenchymal stem cells therapy, clinical perspectives and modification strategies. *Stem Cell Investig.* **6**, 34 (2019).
7. S. Rawal, S. J. Williams, K. Ramachandran, L. Stehno-Bittel, Integration of mesenchymal stem cells into islet cell spheroids improves long-term viability, but not islet function. *Islets* **9**, 87–98 (2017).
8. S. Forbes, A. R. Bond, K. L. Thirlwell, P. Burgoyne, K. Samuel, J. Noble, G. Borthwick, D. Colligan, N. W. A. McGowan, P. S. Lewis, A. R. Fraser, J. C. Mountford, R. N. Carter, N. M. Morton, M. L. Turner, G. J. Graham, J. D. M. Campbell, Human umbilical cord perivascular cells improve human pancreatic islet transplant function by increasing vascularization. *Sci. Transl. Med.* **12**, eaan5907 (2020).
9. S. Schu, M. Nosov, L. O'Flynn, G. Shaw, O. Treacy, F. Barry, M. Murphy, T. O'Brien, T. Ritter, Immunogenicity of allogeneic mesenchymal stem cells. *J. Cell. Mol. Med.* **16**, 2094–2103 (2012).
10. M. J. Crop, S. S. Korevaar, R. De Kuiper, J. N. M. Ijzermans, N. M. Van Besouw, C. C. Baan, W. Weimar, M. J. Hoogduijn, Human mesenchymal stem cells are susceptible to lysis by CD8$^+$ T cells and NK cells. *Cell Transplant.* **20**, 1547–1559 (2011).
11. M. A. Podestà, G. Remuzzi, F. Casiraghi, Mesenchymal stromal cells for transplant tolerance. *Front Immunol.* **10**, 1287 (2019).
12. P.-P. Cheng, X.-C. Liu, P.-F. Ma, C. Gao, J.-L. Li, Y.-Y. Lin, W. Shao, S. Han, B. Zhao, L.-M. Wang, J.-Z. Fu, L.-X. Meng, Q. Li, Q.-Z. Lian, J.-J. Xia, Z.-Q. Qi, iPSC-MSCs combined with low-dose rapamycin induced islet allograft tolerance through suppressing Th1 and enhancing regulatory T-cell differentiation. *Stem Cells Dev.* **24**, 1793–1804 (2015).
13. W. Duan, X. Yu, D. Ma, B. Yang, Y. Li, L. Huang, L. Liu, G. Chen, D. Xu, Y. Ding, Mesenchymal stem cells in combination with low-dose rapamycin significantly prolong islet allograft survival through induction of regulatory T cells. *Biochem. Biophys. Res. Commun.* **506**, 619–625 (2018).
14. W. Ge, J. Jiang, M. L. Baroja, J. Arp, R. Zassoko, W. Liu, A. Bartholomew, B. Garcia, H. Wang, Infusion of mesenchymal stem cells and rapamycin synergize to attenuate alloimmune responses and promote cardiac allograft tolerance. *Am. J. Transplant.* **9**, 1760–1772 (2009).
15. B. Wang, Y. Lin, Y. Hu, W. Shan, S. Liu, Y. Xu, H. Zhang, S. Cai, X. Yu, Z. Cai, H. Huang, mTOR inhibition improves the immunomodulatory properties of human bone marrow mesenchymal stem cells by inducing COX-2 and PGE_2. *Stem Cell Res Ther.* **8**, 292 (2017).
16. J. Zheng, H. Li, L. He, Y. Huang, J. Cai, L. Chen, C. Zhou, H. Fu, T. Lu, Y. Zhang, J. Yao, Y. Yang, Preconditioning of umbilical cord-derived mesenchymal stem cells by rapamycin increases cell migration and ameliorates liver ischaemia/reperfusion injury in mice via the CXCR4/CXCL12 axis. *Cell Prolif.* **52**, e12546 (2018).
17. N. de C. Noronha, A. Mizukami, C. Caliári-Oliveira, J. G. Cominal, J. L. M. Rocha, D. T. Covas, K. Swiech, K. C. R. Malmegrim, Priming approaches to improve the efficacy of mesenchymal stromal cell-based therapies. *Stem Cell Res. Ther.* **10**, 131 (2019).
18. M. Duijvestein, M. E. Wildenberg, M. M. Welling, S. Hennink, I. Molendijk, V. L. van Zuylen, T. Bosse, A. C. W. Vos, E. S. M. de Jonge-Muller, H. Roelofs, L. van der Weerd, H. W. Verspaget, W. E. Fibbe, A. A. te Velde, G. R. van den Brink, D. W. Hommes, Pretreatment with interferon-γ enhances the therapeutic activity of mesenchymal stromal cells in animal models of colitis. *Stem Cells* **29**, 1549–1558 (2011).
19. H. Fan, G. Zhao, L. Liu, F. Liu, W. Gong, X. Liu, L. Yang, J. Wang, Y. Hou, Pre-treatment with IL-1β enhances the efficacy of MSC transplantation in DSS-induced colitis. *Cell. Mol. Immunol.* **9**, 473–481 (2012).
20. H. Zahir, G. McCaughan, M. Gleeson, R. A. Nand, A. J. McLachlan, Factors affecting variability in distribution of tacrolimus in liver transplant recipients. *Br. J. Clin. Pharmacol.* **57**, 298–309 (2004).
21. S. Pathak, S. Acharya, S. Regmi, P. Shrestha, Z. You, Y. K. Bae, M. H. Park, S. Yook, J.-R. Kim, S. Y. Park, D. Jeong, C. S. Yong, J. O. Kim, J. H. Chang, J.-H. Jeong, Particulate-based single-dose local immunosuppressive regimen for inducing tolerogenic dendritic cells in xenogeneic islet transplantation. *Adv. Healthc. Mater.* **10**, e2001157 (2021).
22. N. N. Ng, A. S. Thakor, Locoregional delivery of stem cell-based therapies. *Sci. Transl. Med.* **12**, eaba4564 (2020).
23. M. C. Ciuffreda, G. Malpasso, P. Musarò, V. Turco, M. Gnecchi, Protocols for in vitro differentiation of human mesenchymal stem cells into osteogenic, chondrogenic and adipogenic lineages, in *Mesenchymal Stem Cells*, M. Gnecchi, Ed. (Springer New York, 2016), vol. 1416 of *Methods in Molecular Biology*, pp. 149–158.
24. S. Regmi, J.-H. Jeong, Superiority of three-dimensional stem cell clusters over monolayer culture: An archetype to biological application. *Macromol. Res.* **24**, 1037–1046 (2016).
25. N. Song, M. Scholtemeijer, K. Shah, Mesenchymal stem cell immunomodulation: Mechanisms and therapeutic potential. *Trends Pharmacol. Sci.* **41**, 653–664 (2020).
26. J. Croden, W. Huang, G. R. Rayat, Immune response associated with islet xenotransplantation in small and large animal models. *Xenotransplantation New Insights* 10.5772/intechopen.68999 (2017).
27. V. A. L. Huurman, J. H. L. Velthuis, R. Hilbrands, T. I. M. Tree, P. Gillard, P. M. W. V. D. Meer-Prins, G. Duinkerken, G. G. M. Pinkse, B. Keymeulen, D. L. Roelen, F. H. J. Claas, D. G. Pipeleers, B. O. Roep, Allograft-specific cytokine profiles associate with clinical outcome after islet cell transplantation. *Am. J. Transplant.* **9**, 382–388 (2009).
28. S. Lacotte, S. Borot, S. Ferrari-Lacraz, J. Villard, S. Demuylder-Mischler, G. Oldani, P. Morel, G. Mentha, T. Berney, C. Toso, Posttransplant cellular immune reactivity against donor

antigen correlates with clinical islet transplantation outcome: Towards a better posttransplant monitoring. *Cell Transplant.* **21**, 2339–2350 (2012).
29. N. C. Schloot, P. Hanifi-Moghaddam, C. Goebel, S. V. Shatavi, S. Flohé, H. Kolb, H. Rothe, Serum IFN-γ and IL-10 levels are associated with disease progression in non-obese diabetic mice. *Diabetes Metab. Res. Rev.* **18**, 64–70 (2002).
30. A. O. Kamphorst, R. Ahmed, Manipulating the PD-1 pathway to improve immunity. *Curr. Opin. Immunol.* **25**, 381–388 (2013).
31. G. Pennesi, PD1-mediated mesenchymal stem cells immunemodulation: The two sides of the coin. *Int. Clin. Pathol. J.* **6**, 164–165 (2018).
32. M. Saresella, V. Rainone, N. M. Al-Daghri, M. Clerici, D. Trabattoni, The PD-1/PD-L1 pathway in human pathology. *Curr. Mol. Med.* **12**, 259–267 (2012).
33. N. Kojima, S. Takeuchi, Y. Sakai, Rapid aggregation of heterogeneous cells and multiple-sized microspheres in methylcellulose medium. *Biomaterials* **33**, 4508–4514 (2012).
34. F. Tao, H. Mihara, N. Kojima, in *Hepatic Stem Cells*, N. Tanimizu, Ed. (Springer New York, 2019), vol. 1905 of *Methods in Molecular Biology*, pp. 157–165.
35. A. M. Bratt-Leal, A. H. Nguyen, K. A. Hammersmith, A. Singh, T. C. McDevitt, A microparticle approach to morphogen delivery within pluripotent stem cell aggregates. *Biomaterials* **34**, 7227–7235 (2013).
36. C. C. Ahrens, Z. Dong, W. Li, Engineering cell aggregates through incorporated polymeric microparticles. *Acta Biomater.* **62**, 64–81 (2017).
37. O. Qutachi, K. M. Shakesheff, L. D. K. Buttery, Delivery of definable number of drug or growth factor loaded poly(dl-lactic acid-co-glycolic acid) microparticles within human embryonic stem cell derived aggregates. *J. Control. Release* **168**, 18–27 (2013).
38. S. Regmi, Y. Seo, J.-S. Ahn, S. Pathak, S. Acharya, T. T. Nguyen, S. Yook, J.-H. Sung, J.-B. Park, J. O. Kim, C. S. Young, H.-S. Kim, J.-H. Jeong, Heterospheroid formation improves therapeutic efficacy of mesenchymal stem cells in murine colitis through immunomodulation and epithelial regeneration. *Biomaterials* **271**, 120752 (2021).
39. K. Zhu, Y. Yu, Y. Cheng, C. Tian, G. Zhao, Y. Zhao, All-aqueous-phase microfluidics for cell encapsulation. *ACS Appl. Mater. Interfaces* **11**, 4826–4832 (2019).
40. S. L. Ham, E. Atefi, D. Fyffe, H. Tavana, Robotic production of cancer cell spheroids with an aqueous two-phase system for drug testing. *J. Vis. Exp.* e52754 (2015).
41. S. Suryaprakash, Y.-H. Lao, H.-Y. Cho, M. Li, H. Y. Ji, D. Shao, H. Hu, C. H. Quek, D. Huang, R. L. Mintz, J. R. Bagó, S. D. Hingtgen, K.-B. Lee, K. W. Leong, Engineered mesenchymal stem cell/nanomedicine spheroid as an active drug delivery platform for combinational glioblastoma therapy. *Nano Lett.* **19**, 1701–1705 (2019).
42. J. Li, S. G. Kim, J. Blenis, Rapamycin: One drug, many effects. *Cell Metabolism.* **19**, 373–379 (2014).
43. D.-W. Kim, K. Y. Weon, Pharmaceutical application and development of fixed-dose combination: Dosage form review. *J. Pharm. Investig.* **51**, 555–570 (2021).
44. K.-W. Kim, S.-J. Moon, M.-J. Park, B.-M. Kim, E.-K. Kim, S.-H. Lee, E.-J. Lee, B.-H. Chung, C.-W. Yang, M.-L. Cho, Optimization of adipose tissue-derived mesenchymal stem cells by rapamycin in a murine model of acute graft-versus-host disease. *Stem Cell Res Ther.* **6**, 202 (2015).
45. L. Gao, S. Cen, P. Wang, Z. Xie, Z. Liu, W. Deng, H. Su, X. Wu, S. Wang, J. Li, Y. Ouyang, Y. Wu, H. Shen, Autophagy improves the immunosuppression of CD4+ T cells by mesenchymal stem cells through transforming growth factor-β1. *Stem Cells Transl. Med.* **5**, 1496–1505 (2016).
46. M. E. Castro-Manrreza, J. J. Montesinos, Immunoregulation by mesenchymal stem cells: Biological aspects and clinical applications. *J. Immunol. Res.* **2015**, 1–20 (2015).
47. S. Regmi, S. Pathak, J. O. Kim, C. S. Yong, J.-H. Jeong, Mesenchymal stem cell therapy for the treatment of inflammatory diseases: Challenges, opportunities, and future perspectives. *Eur. J. Cell Biol.* **98**, 151041 (2019).
48. K. M. van Megen, E.-J. T. van't Wout, J. L. Motta, B. Dekker, T. Nikolic, B. O. Roep, Activated mesenchymal stromal cells process and present antigens regulating adaptive immunity. *Front. Immunol.* **10**, 694 (2019).
49. L.-C. Chen, H.-W. Wang, C.-C. Huang, Modulation of inherent niches in 3D multicellular MSC spheroids reconfigures metabolism and enhances therapeutic potential. *Cell* **10**, 2747 (2021).
50. A. H. Sharpe, K. E. Pauken, The diverse functions of the PD1 inhibitory pathway. *Nat. Rev. Immunol.* **18**, 153–167 (2018).
51. S. Tipnis, C. Viswanathan, A. S. Majumdar, Immunosuppressive properties of human umbilical cord-derived mesenchymal stem cells: Role of B7-H1 and IDO. *Immunol. Cell Biol.* **88**, 795–806 (2010).
52. L. C. Davies, N. Heldring, N. Kadri, K. Le Blanc, Mesenchymal stromal cell secretion of programmed death-1 ligands regulates T cell mediated immunosuppression. *Stem Cells* **35**, 766–776 (2017).
53. C. L. Stabler, Y. Li, J. M. Stewart, B. G. Keselowsky, Engineering immunomodulatory biomaterials for type 1 diabetes. *Nat. Rev. Mater.* **4**, 429–450 (2019).
54. A. Hamann, A. Nguyen, A. K. Pannier, Nucleic acid delivery to mesenchymal stem cells: A review of nonviral methods and applications. *J. Biol. Eng.* **13**, 7 (2019).
55. J. Xu, J. Li, S. Lin, T. Wu, H. Huang, K. Zhang, Y. Sun, K. W. K. Yeung, G. Li, L. Bian, Nanocarrier-mediated codelivery of small molecular drugs and siRNA to enhance chondrogenic differentiation and suppress hypertrophy of human mesenchymal stem cells. *Adv. Funct. Mater.* **26**, 2463–2472 (2016).
56. D. Wen, Y. Peng, D. Liu, Y. Weizmann, R. I. Mahato, Mesenchymal stem cell and derived exosome as small RNA carrier and Immunomodulator to improve islet transplantation. *J. Control. Release* **238**, 166–175 (2016).
57. D. Y.-W. Lin, Y. Tanaka, M. Iwasaki, A. G. Gittis, H.-P. Su, B. Mikami, T. Okazaki, T. Honjo, N. Minato, D. N. Garboczi, The PD-1/PD-L1 complex resembles the antigen-binding Fv domains of antibodies and T cell receptors. *Proc. Natl. Acad. Sci. U.S.A.* **105**, 3011–3016 (2008).
58. C. Viricel, M. Ahmed, K. Barakat, Human PD-1 binds differently to its human ligands: A comprehensive modeling study. *J. Mol. Graph. Model.* **57**, 131–142 (2015).
59. K. Magiera-Mularz, J. Kocik, B. Musielak, J. Plewka, D. Sala, M. Machula, P. Grudnik, M. Hajduk, M. Czepiel, M. Siedlar, T. A. Holak, L. Skalniak, Human and mouse PD-L1: Similar molecular structure, but different druggability profiles. *iScience* **24**, 101960 (2021).
60. M. M. Coronel, K. E. Martin, M. D. Hunckler, G. Barber, E. B. O'Neill, J. D. Medina, E. Opri, C. A. McClain, L. Batra, J. D. Weaver, H. S. Lim, P. Qiu, E. A. Botchwey, E. S. Yolcu, H. Shirwan, A. J. García, Immunotherapy via PD-L1-presenting biomaterials leads to long-term islet graft survival. *Sci Adv.* **6**, eaba5573 (2020).
61. K. Akiyama, C. Chen, D. Wang, X. Xu, C. Qu, T. Yamaza, T. Cai, W. Chen, L. Sun, S. Shi, Mesenchymal-stem-cell-induced immunoregulation involves FAS-ligand-/FAS-mediated T cell apoptosis. *Cell Stem Cell* **10**, 544–555 (2012).
62. T. Gaber, K. Schönbeck, H. Hoff, C. L. Tran, C. Strehl, A. Lang, S. Ohrndorf, M. Pfeiffenberger, E. Röhner, G. Matziolis, G.-R. Burmester, F. Buttgereit, P. Hoff, CTLA-4 mediates inhibitory function of mesenchymal stem/stromal cells. *Int J Mol Sci.* **19**, 2312 (2018).
63. X. Liu, Engineering beta-cell spheroids for type 1 diabetes treatment (*All Dissertations*, 2013); https://tigerprints.clemson.edu/all_dissertations/1225.
64. A. R. Pepper, A. Bruni, A. M. J. Shapiro, Clinical islet transplantation: Is the future finally now? *Curr. Opin. Organ Transplant.* **23**, 428–439 (2018).
65. J. Paez-Mayorga, S. Capuani, N. Hernandez, M. Farina, C. Y. X. Chua, R. Blanchard, A. Sizovs, H.-C. Liu, D. W. Fraga, J. A. Niles, H. F. Salazar, B. Corradetti, A. G. Sikora, M. Kloc, X. C. Li, A. O. Gaber, J. E. Nichols, A. Grattoni, Neovascularized implantable cell homing encapsulation platform with tunable local immunosuppressant delivery for allogeneic cell transplantation. *Biomaterials* **257**, 120232 (2020).
66. T. T. Nguyen, T. T. Pham, H. T. Nguyen, M. R. Nepal, C. D. Phung, Z. You, N. Katila, N. T. Pun, T. C. Jeong, D.-Y. Choi, P.-H. Park, C. S. Yong, J. O. Kim, S. Yook, J.-H. Jeong, Engineering "cell-particle hybrids" of pancreatic islets and bioadhesive FK506-loaded polymeric microspheres for local immunomodulation in xenogeneic islet transplantation. *Biomaterials* **221**, 119415 (2019).
67. M. Li, L. M. Kaminskas, N. Marasini, Recent advances in nano/microparticle-based oral vaccines. *J. Pharm. Investig.* **51**, 425–438 (2021).
68. J. H. Jung, S. G. Jin, Microneedle for transdermal drug delivery: Current trends and fabrication. *J. Pharm. Investig.* **51**, 503–517 (2021).
69. T. T. Nguyen, J. Jeong, Development of a single-jet electrospray method for producing quercetin-loaded poly (lactic-co-glycolic acid) microspheres with prolonged-release patterns. *J. Drug Deliv. Sci. Technol.* **47**, 268–274 (2018).
70. P. Anderson, A. B. Carrillo-Gálvez, F. Martín, Isolation of murine adipose tissue-derived mesenchymal stromal cells (mASCs) and the analysis of their proliferation in vitro. *Bio-protocol* **5**, e1642 (2015).
71. G. Yu, X. Wu, G. Kilroy, Y.-D. C. Halvorsen, J. M. Gimble, Z. E. Floyd, Isolation of murine adipose-derived stem cells. *Methods Mol. Biol.* **702**, 29–36 (2011).
72. C. Heckman, S. Kanagasundaram, M. Cayer, J. Paige, Preparation of cultured cells for scanning electron microscope. *Protocol Exchange* 10.1038/nprot.2007.504, (2007).
73. T. T. Nguyen, F. Emami, S. Yook, H. T. Nguyen, T. T. Pham, S. Pathak, S. Regmi, J. O. Kim, C. S. Yong, J.-R. Kim, J.-H. Jeong, Local release of NECA (5′-(N-ethylcarboxamido) adenosine) from implantable polymeric sheets for enhanced islet revascularization in extrahepatic transplantation site. *J. Control. Release* **321**, 509–518 (2020).
74. P. Shrestha, S. Regmi, J.-H. Jeong, Injectable hydrogels for islet transplantation: A concise review. *J. Pharm. Investig.* **50**, 29–45 (2020).

Acknowledgments: We thank the Core Research Support Center for Natural Products and Medical Materials (CRCNM, Yeungnam University, Republic of Korea) for technical support.
Funding: This research was supported by the National Research Foundation of Korea (NRF) funded by the Ministry of Science and ICT (grant nos. 2020R1C1C1004733 and 2021K1A3A1A20002609), by the Cooperative Research Program for Agriculture Science and Technology Development Rural Development Administration (grant no. PJ015596), by the Bio and Medical Technology Development Program of the NRF and funded by the Korean government (MSIT) (grant no. 2022M3A9G8017220), and by the Korean Fund for Regenerative

Medicine (KFRM) grant funded by the Ministry of Science and ICT, the Ministry of Health & Welfare (grant no. 22A0205L1). **Author contributions:** T.T.N. and J.-H.J. were responsible for study conception and design. D.-V.P., C.D.P., and P.-H.P. contributed to acquisition of RT-PCR data. M.R.N. and T.C.J. contributed to acquisition of LC-MS/MS data. M.P., Y.S., M.J., J.-R.K., and J.-H.C. contributed to acquisition of flow cytometry data. D.-Y.C. provided the microtome tool for histological study. I.-K.K. provided and characterized GFP-expressing MSCs. J.-H.K., C.S.Y., J.O.K., J.-H.S., H.-L.J., H.-S.K., J.P., and M.S. contributed to revision of the manuscript. J.-H.J. and S.Y. supervised, wrote, revised, and edited the manuscript. **Competing interests:** The authors declare that they have no competing interests. **Data and materials availability:** All data needed to evaluate the conclusions in the paper are present in the paper and/or the Supplementary Materials.

Submitted 6 January 2022
Accepted 11 July 2022
Published 24 August 2022
10.1126/sciadv.abn8614